Journal of Geophysical Research: Solid Earth

RESEARCH ARTICLE
10.1029/2018JB016056

Crack Models of Repeating Earthquakes Predict Observed Moment-Recurrence Scaling

C. Cattania[1,2] and P. Segall[1]

[1]Department of Geophysics, Stanford University, Stanford, CA, USA, [2]Institute of Earth and Environmental Science, University of Potsdam, Potsdam, Germany

Key Points:
- We derive analytical expressions for recurrence interval and stress drop of events on circular asperities in creeping faults
- The theory produces the observed scaling between recurrence interval and seismic moment of repeating earthquakes
- We predict and quantify a break in self-similarity and decrease in stress drops close to the nucleation dimension

Correspondence to:
C. Cattania,
camcat@stanford.edu

Citation:
Cattania, C., & Segall, P. (2018). Crack models of repeating earthquakes predict observed moment-recurrence scaling. *Journal of Geophysical Research: Solid Earth*, *123*. https://doi.org/10.1029/2018JB016056

Received 3 MAY 2018
Accepted 9 NOV 2018
Accepted article online 14 NOV 2018

Abstract Small repeating earthquakes are thought to represent rupture of isolated asperities loaded by surrounding creep. The observed scaling between recurrence interval and seismic moment, $T_r \sim M^{1/6}$, contrasts with expectation assuming constant stress drop and no aseismic slip ($T_r \sim M^{1/3}$). Here we demonstrate that simple crack models of velocity-weakening asperities in a velocity-strengthening fault predict the $M^{1/6}$ scaling; however, the mechanism depends on asperity radius, R. For small asperities ($R_\infty < R < 2R_\infty$, where R_∞ is the nucleation radius) numerical simulations with rate-state friction show interseismic creep penetrating inward from the edge, and earthquakes nucleate in the center and rupture the entire asperity. Creep penetration accounts for ~25% of the slip budget, the nucleation phase takes up a larger fraction of slip. Stress drop increases with increasing R; the lack of self-similarity being due to the finite nucleation dimension. For $2R_\infty < R \lesssim 6R_\infty$ simulations exhibit simple cycles with ruptures nucleating from the edge. Asperities with $R \gtrsim 6R_\infty$ exhibit complex cycles of partial and full ruptures. Here T_r is explained by an energy criterion: full rupture requires that the energy release rate everywhere on the asperity at least equals the fracture energy, leading to the scaling $T_r \sim M^{1/6}$. Remarkably, in spite of the variability in behavior with source dimension, the scaling of T_r with stress drop $\Delta\tau$, nucleation length and creep rate v_{pl} is the same across all regimes: $T_r \sim \sqrt{R_\infty}\Delta\tau^{5/6}M_0^{1/6}/v_{pl}$. This supports the use of repeating earthquakes as creepmeters and provides a physical interpretation for the scaling observed in nature.

Plain Language Summary While most earthquake sequences have complex temporal patterns, some small earthquakes are quite predictable: they repeat periodically. The time between consecutive events (recurrence interval) grows with earthquake size: as intuitive, it takes longer to accumulate the mechanical energy for large earthquakes. However, the scaling between the recurrence interval and earthquake energy (seismic moment) is not what simple physical considerations predict. It is often assumed that faults are locked between events and seismic slip must therefore keep up with long-term plate motion. This leads to the scaling: $T_r \sim M_0^{1/3}$, but the observed scaling is $T_r \sim M_0^{1/6}$. In fact, faults are not fully locked between earthquakes: they can slip slowly, or release part of the energy in smaller quakes between the larger ones. Here we use numerical simulations, and ideas from fracture mechanics, to understand what controls the time between repeating quakes. The main results are (1) analytical expressions of the recurrence interval as a function of earthquake size, predicting the observed scaling; (2) explanation of the differences between the cycle of small and large earthquakes (fraction of slow slip, direction of rupture propagation, and the occurrence of smaller quakes between large ones) and the quantities determining these transitions.

1. Introduction

Unlike large earthquakes, small quakes can be very predictable; periodic sequences of events with very similar waveforms have been detected in multiple locations worldwide. They are typically understood as the rupture of locked patches surrounded by aseismic creep, loading them at a usually constant rate. An interesting observation is the scaling between their recurrence interval and seismic moment. Nadeau and Johnson (1998) observed that the recurrence interval T_r and seismic moment M_0 scale as $T \sim M_0^{1/6}$ for small repeaters on the San Andreas fault, and subsequent studies confirmed this scaling in other areas (Chen et al., 2007). As outlined by Nadeau and Johnson (1998), standard scaling arguments predict that $T_r \sim M_0^{1/3}$. Assuming constant stress drop constrains seismic slip to be linear with rupture dimension ($S \sim R$); further assuming that the coseismic slip is equal to the slip deficit accumulated since the previous event ($S = v_{pl}T_r$, where v_{pl} is fault slip rate) results

in a linear scaling between recurrence interval T_r and R. Since $M_0 \sim \Delta\sigma R^3$ a constant stress drop $\Delta\sigma$ implies $T_r \sim M_0^{1/3}$. Nadeau and Johnson (1998) explained the observed scaling by abandoning the constant stress drop assumption, inferring $\Delta\sigma \sim M_0^{-1/4}$. To fit observations, very high stress drops (of the order of 10^3–10^4 MPa) are required for the smallest events. Alternatively, the scaling can be explained by assuming constant $\Delta\sigma$ but relaxing the assumption that $S = v_{pl}T_r$, that is, by not assuming that the fault is entirely locked interseismically so that the coseismic slip is less than $v_{pl}T_r$. This was suggested by Beeler et al. (2001), who adopted a strain-hardening rheology on a circular patch experiencing spatially uniform interseismic creep. According to their model, smaller asperities release a large fraction of slip aseismically, which can result in the observed scaling. Similar conclusions were reached by Chen and Lapusta (2009), who presented numerical simulations of seismic cycles on circular, velocity-weakening asperities surrounded by a velocity-strengthening exterior. They found that smaller asperities experience a larger fraction of aseismic slip, as suggested by Beeler et al. (2001). Alternatively, Sammis and Rice (2001) proposed a geometrical explanation: asperities at the transition between locked and creeping regions experience a stress field decaying with distance from the transition, which under certain assumptions results in $T_r \sim M_0^{1/6}$. Because of the particular geometry, this may be less generally applicable than the aseismic slip interpretation.

Here we seek a deeper understanding of the factors that control the recurrence interval of earthquakes on circular asperities using fracture mechanics concepts, guided by numerical simulations of faults obeying rate-state friction. Chen and Lapusta (2009) demonstrated that numerical simulations of velocity-weakening asperities embedded in a velocity-strengthening fault reproduce the $T_r \sim M_0^{1/6}$ scaling. They attributed this observation to the occurrence of creep, which is significant on asperities with a dimension close to the nucleation size. Here we start from a similar set of numerical simulations and derive analytical expressions for the recurrence interval. Our goal is twofold: first, by formulating the problem in terms of physical quantities such as stress drop and nucleation length, we develop a model which can be applied to a different choice or parameters or even a potentially different frictional behavior. Second, we explore the behavior of asperities much larger than the nucleation dimension, which do not experience significant aseismic slip. In this regime, we provide a different physical explanation for the observed scaling. The seismic moment of a circular crack of radius R with uniform stress drop $\Delta\sigma$ is (Eshelby, 1957)

$$M_0 = \frac{16}{7}\Delta\sigma R^3 \tag{1}$$

For constant stress drop, the scaling $T_r \sim M_0^{1/6}$ implies that $T_r \sim R^{1/2}$. Interestingly, this is analogous to the scaling derived by Werner and Rubin (2013) for antiplane faults, by considering the balance between the energy release rate for a crack loaded by downdip creep and the fracture energy absorbed to propagate the crack through the full velocity-weakening region, and confirmed by Kato (2012a) for subduction zones. Here we demonstrate that, under certain assumptions, this energy argument applied to circular asperities leads to the same scaling for circular cracks. However, numerical simulations only exhibit this scaling above a critical radius (twice the nucleation radius R_∞, defined below), and stress drop is not constant for asperities smaller than this dimension. We develop crack models to answer the following questions: (1) How long does it take for creep loading to nucleate a dynamic rupture? (2) Once an event nucleates, under what conditions will it rupture the entire asperity? (3) How does stress drop vary with asperity dimension? We find that the answers to these questions depend on the asperity dimension R relative to R_∞. This is perhaps not surprising, since this dimension controls the transition between aseismic and seismic slip; the occurrence of creep affects the strength of the asperity and hence rupture propagation. Furthermore, as R decreases toward R_∞, the assumptions behind classical seismological models of circular ruptures break down: the rupture cannot be assumed to start at a point expanding subsequently at seismic rupture velocities. In this limit, the rupture is not self similar and the stress drop increases slightly with R. Combining these results, we obtain analytical estimates for the recurrence interval as a function of asperity radius R, which predict a scaling close to that observed in nature. In summary, we show that T_r scales approximately with $M_0^{1/6}$ over a range of asperity radii, and potentially also for $R \gg R_\infty$; however, the underlying physics differs depending on asperity size.

2. Numerical Simulations

In order to test the analytical results derived in the next section, we ran a set of simulations analogous to those presented by Chen and Lapusta (2009): a circular velocity-weakening asperity on an otherwise velocity-strengthening planar fault. Here we use the quasi-dynamic rupture code *FDRA* (Mavrommatis et al.,

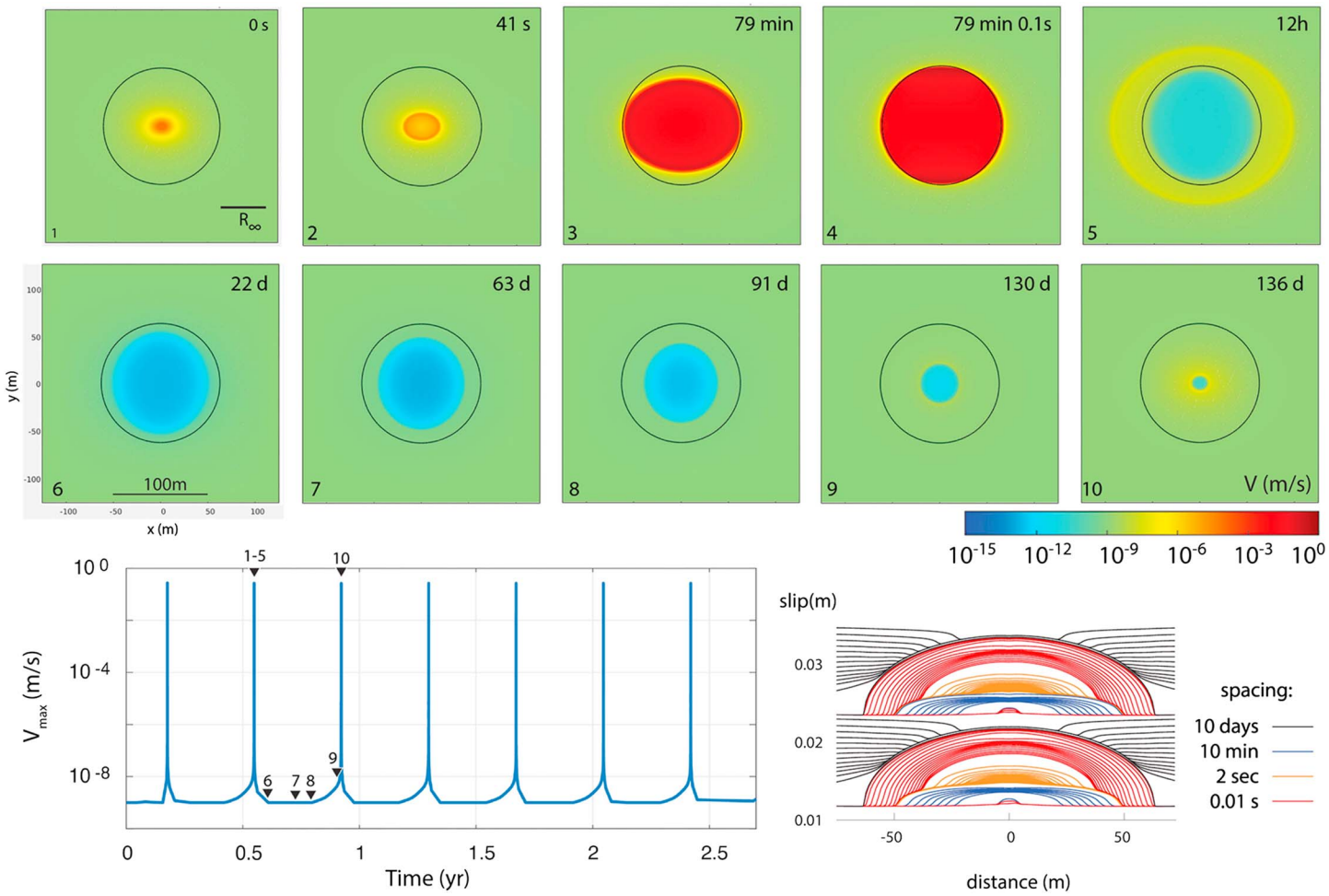

Figure 1. (top) Full rupture on an asperity of size $R = 16L_b$ ($1.3R_\infty$). Color is slip speed; slip is in the x direction. The time since the arrival of the creep front at $r = 0$ is indicated; notice the acceleration in panels (1) and (2) preceding the main event. (bottom left) Maximum slip velocity in the VW region versus time, showing that this fault experiences periodic seismic ruptures. Numbers refer to the snapshots above. (bottom right) Slip history over two cycles. Red lines indicate the seismic phase ($v > v_{dyn}$); blue and orange lines indicate slip between the arrival of the creep front and the onset of the seismic phase; black lines indicate interseismic slip.

2017; Segall & Bradley, 2012). The agreement between our simulation results and the fully dynamic models used by Chen and Lapusta (2009) and the success of our quasi-static derivations in reproducing the observed scaling indicate that dynamic effects are not essential in determining the recurrence interval scaling.

The frictional resistance on the fault τ_f is controlled by rate-state friction (Dieterich, 1978):

$$\tau_f(v,\theta) = \sigma\left[f_0 + a\log\frac{v}{v_0} + b\log\frac{\theta v_0}{d_c}\right], \tag{2}$$

where σ is the effective normal stress; a and b are constitutive parameters; d_c is the rate-state slip-weakening distance (a characteristic sliding length over which state θ evolves). The parameters v and v_0 are the slip velocity and reference slip velocity; f_0 is the steady state friction coefficient at $v = v_0$, and θ is a state variable which here evolves according to the aging law (Ruina, 1983):

$$\frac{\mathrm{d}\theta}{\mathrm{d}t} = 1 - \frac{\theta v}{d_c}, \tag{3}$$

so that the steady state strength at constant slip velocity v is given by

$$\tau_{ss}(v) = \sigma\left[f_0 + (a-b)\log\frac{v}{v_0}\right]. \tag{4}$$

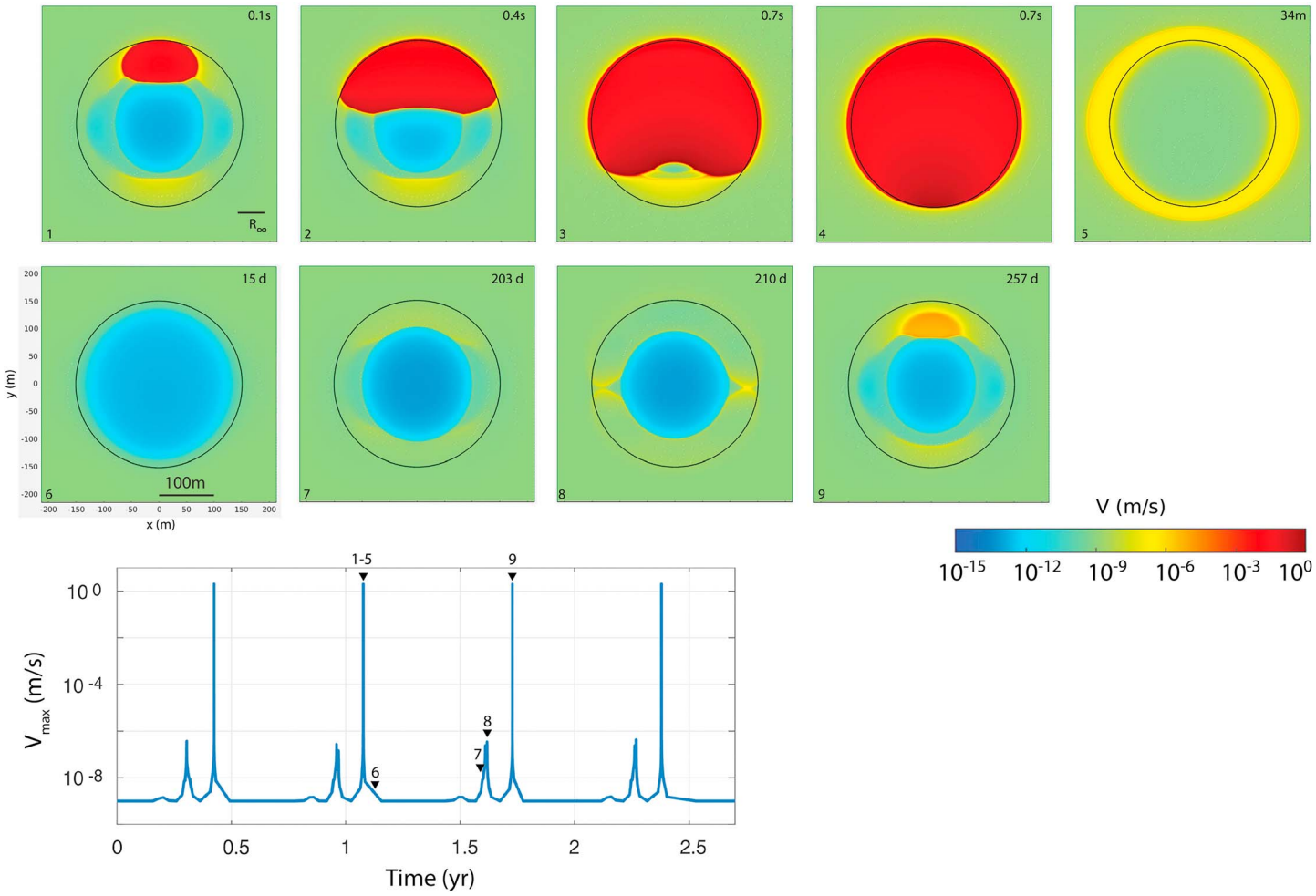

Figure 2. Example of a seismic cycle on an asperity with $R = 38L_b$ ($3R_\infty$). Color is slip speed. (top) Seismic event (panels 1–4) and afterslip (panel 5). Inward propagation of a creep front, and a slip acceleration that does not reach seismic velocity (panel 8). The time from the onset of the earthquake is indicated. (bottom) Maximum slip velocity in the VW region versus time, showing seismic and aseismic slip episodes. Numbers refer to the panels above.

Chen (2012) ran simulations with another commonly used state evolution law (the slip law) and showed that the scaling between recurrence interval and moment ($T_r \sim M_0^{1/6}$) is unchanged.

Slip on the fault is controlled by the following equation of motion:

$$\tau_{\text{el}}(\mathbf{x}) - \tau_f(\mathbf{x}) = \frac{\mu}{2c_s} v(\mathbf{x}), \tag{5}$$

where μ is the shear modulus and τ_{el} is the elastostatic shear stress due to loading from the boundary and quasi-static elastic interactions between fault elements computed through a Boundary Element Method approach. The right-hand side represents radiation damping, which accounts for the stress change due to radiation of plane *S* waves (Rice, 1993), with c_s as the shear wave speed.

Rate-state friction combined with elasticity leads to characteristic dimensions which control earthquake nucleation, and the transition between seismic and aseismic behavior. One such dimension is

$$L_b = \frac{\mu' d_c}{\sigma b}. \tag{6}$$

where $\mu' = \mu$ for antiplane shear and $\mu/(1-\nu)$, with ν = Poisson's ratio, for plane strain deformation. This length scale was first identified by Dieterich (1992) as the minimum nucleation length, although subsequent studies obtained different estimates (Rubin & Ampuero, 2005, and references therein). For nominal calcula-

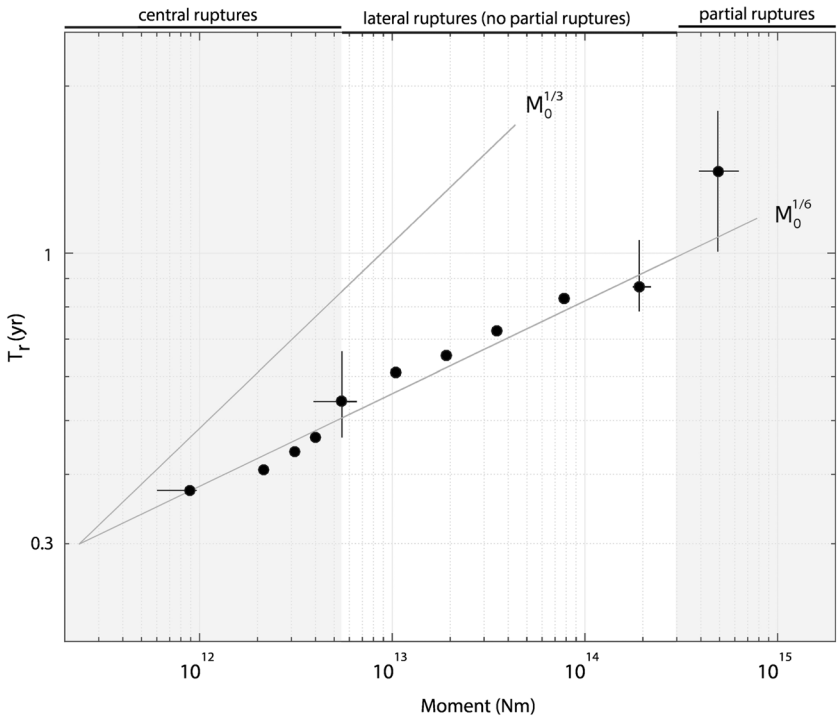

Figure 3. Scaling of T_r with seismic moment from numerical simulations. The y axis is the time since the last rupture; we define T_r as the time between consecutive full ruptures. Error bars indicate range of observed T_r; the large variation for the fifth data point is due to alternation of central and lateral ruptures.

tions we set $\mu = 30$ GPa, $\nu = 0.25$, $d_c = 0.1$ mm, $b = 0.02$ and $a - b = \pm 0.005$ for the velocity-strengthening and velocity-weakening region respectively, resulting in $L_b = 4$m), but later vary a/b. We tested asperity radii R such that R/L_b is between 6 and 100. The system is driven by imposed velocity $v = v_{\text{pl}}$ (10^{-9} m/s) outside the domain, which has a size of $6R$ in each direction. As long as the domain boundaries are sufficiently far, the domain size has little influence of the simulation results: we tested sizes between $6R$ and $100R$ and found a variation of less than 1% in recurrence interval. We define earthquakes as the period during which the slip velocity at any point exceeds the threshold velocity $v_{\text{dyn}} = 2a\sigma c_s/\mu'$ (here 0.14 m/s) at which point the inertial term in equation 5 becomes significant (Rubin & Ampuero, 2005).

The rupture behavior as a function or R is described in detail in Chen and Lapusta (2009); here we summarize the main results. The smallest faults ($R \leq 12.5L_b$) are entirely aseismic. However, they also exhibit cycles: most slip takes place during short episodes of slip at a rate higher than loading rate (e.g., $v \sim 10^3 v_{\text{pl}}$ for the smallest fault, $R = 6L_b$), and are nearly locked between such events. Intermediate size asperities ($15.7L_b \leq R \leq 20.5L_b$) exhibit cycles of seismic ruptures nucleating at the center of the asperity (Figure 1). After each rupture, a creep front propagates inward from the edge and the next rupture occurs when the front reaches the center. For larger asperities ($R \geq 25L_b$) ruptures nucleate from the side, when the creep front has only partially penetrated the asperity. There are always one or more transient aseismic slip events in each cycle before reaching seismic velocities (Figure 2). For $R \simeq 22L_b$, central and lateral ruptures alternate. Finally, we note that on the largest asperity tested ($R = 100L_b$) some seismic ruptures arrest before covering the entire asperity; we denote these as partial ruptures. In section 3.4, we further explore the partial ruptures regime by choosing rate-state parameters such that similar behavior can be reproduced with lower computational costs. As expected, our simulations result in the $T_r \sim M_0^{1/6}$ scaling observed by Chen and Lapusta (2009; Figure 3), across all the regimes of seismic ruptures described above. However, Figure 4 shows that the scaling between T_r and R varies with asperity radius. For seismic ruptures nucleating at the center, $T_r \sim R$; whereas on asperities with lateral ruptures $T_r \sim R^{1/2}$ (consistent with $T_r \sim M_0^{1/6}$ scaling and constant stress drop). Aseismic events have shorter T_r compared to seismic central ruptures. In the following sections, we develop crack models to understand the scaling of T_r with R (section 3) and the variation of stress drop with asperity dimension (section 4).

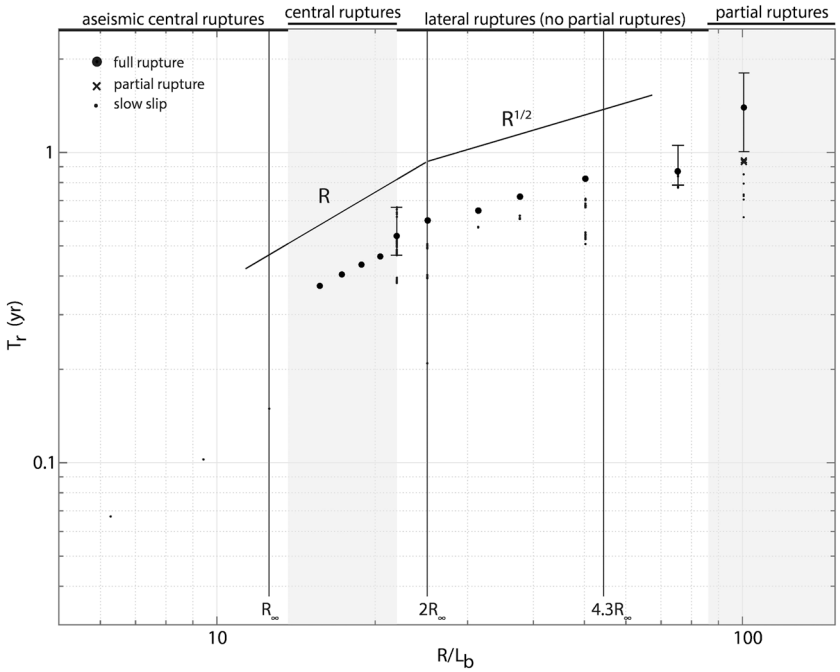

Figure 4. Scaling of T_r with asperity radius. For aseismic events, we define T_r as the time between peaks in slip velocity. We denote as *slow slip* brief slow slip events such as those in Figure 2.

3. Estimating $T_r(R)$ From Crack Models

We estimate the recurrence interval by treating aseismic and seismic slip on the asperity as cracks and determine their propagation or arrest based on energy balance concepts (e.g., Freund, 1990; Griffith, 1921). This approach is analogous to the estimation of the critical nucleation length by Rubin and Ampuero (2005) and to the estimation or recurrence interval on vertical antiplane faults by Werner and Rubin (2013). As shown by Irwin (1957), these energy criteria can be expressed in terms of stress intensity factors (SIF). We consider the following contributions to the SIF, K: (1) K_l, the SIF of a stress-free crack subject to external loading (creep surrounding the asperity); (2) $K_{\Delta\tau}$, the SIF due to changes in stress within the crack due to the variation in strength with slip velocity. A crack can grow if the total SIF is at least equal to the toughness K_c:

$$K_l + K_{\Delta\tau} \geq K_c, \tag{7}$$

which is related to the fracture energy G_c by

$$K_c = \sqrt{2\mu' G_c} \tag{8}$$

following the convention of Tada et al. (2000). We use this framework to model two phases of slip on the fault: the interseismic inward propagation of the creep front, and the propagation or arrest of a seismic rupture. Equation (7) takes on two limiting cases: considering inward growth of the creeping zone, the slip speed immediately behind the crack tip is small (e.g., close to plate rate), thus the fracture energy, and hence K_c, is small, and $K_l \simeq -K_{\Delta\tau}$. On the other hand, considering the energy balance during a full seismic cycle, the total stress change $\Delta\tau = 0$ and equation (7) becomes $K_l = K_c$ (this is the argument introduced by Werner & Rubin, 2013, to estimate T_r for vertical antiplane faults). As shown in the following section, these processes define two time scales: the time required for nucleation (T_{nucl}), and the time when a rupture can propagate over the full asperity (T_{full}).

3.1. Small Asperities (Central Ruptures)

First, we consider asperities small enough that the creep front reaches the center. Figures 5a and 5b show the propagation of the creep front for asperities of different sizes: Figure 5b shows that the lines collapse to

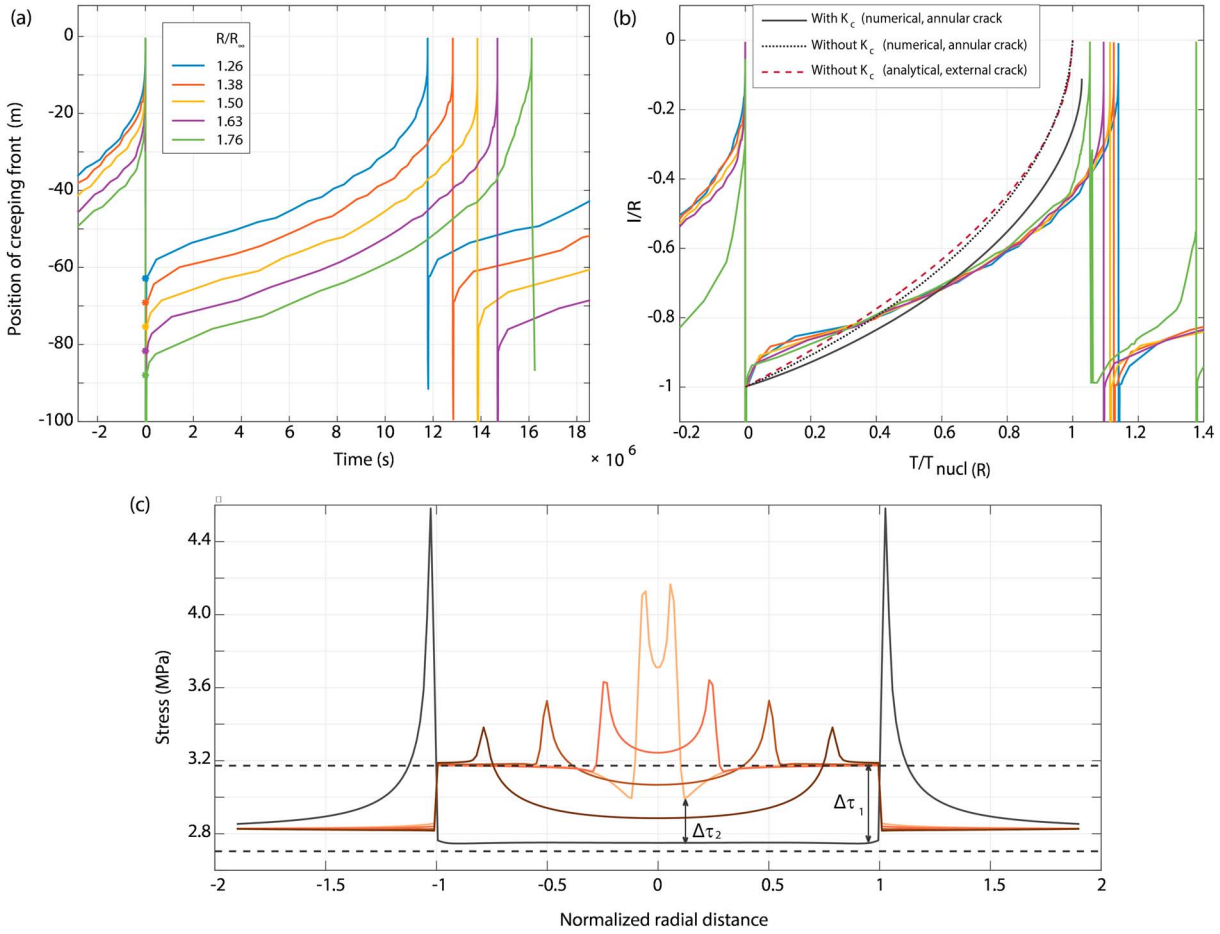

Figure 5. (a) Interseismic propagation of creeping front from the edge of the asperity (indicated by the circle) to the center, estimated from peak stresses. The vertical lines are seismic ruptures. (b) Same plot, with the *y* axis normalized by asperity radius and the *x* axis normalized by equation (9). The black lines are the expected propagation of the front (see text), the red dashed line is the approximate solution derived in Appendix A. (c) Stress profiles as the creep front propagates inward. $\Delta\tau_1$ is the difference between residual stress after an earthquake ($\tau_{ss}(v_{co})$ and ($\tau_{ss}(v_{pl})$), shown by the horizontal dashed lines. As the creep front approaches $r = 0$, the slip velocity exceeds v_{pl} and the stress difference decreases ($\Delta\tau_2$).

the same curve when both position and distance are normalized by a factor proportional to *R*. In Appendix A, we estimate the equation of motion for the creep front by numerically solving equation (7) for an annular crack, with stress change given by the increase from a residual steady state stress at coseismic slip speed $\tau_{ss}(v_{co})$ to steady state friction at the fault slip rate $\tau_{ss}(v_{pl})$, that is $\Delta\tau = \tau_{ss}(v_{pl}) - \tau_{ss}(v_{co})$, see Figure 5c. The black and dotted lines in Figure 5b are the expected position of the front, with and without the contribution from fracture energy. Overall, this model explains the creeping front propagation reasonably well, with a few differences: (1) early in the cycle, the creeping front propagates faster than expected, due to afterslip in the velocity-strengthening region loading the fault faster than plate velocity; (2) toward the end of the cycle, the crack slips faster than expected, due to stressing from the opposing creep front, while our model assumes creep at $v = v_{pl}$. In Appendix A we find that, neglecting fracture energy, the time required for creep to reach the center and nucleate a rupture is

$$T_{nucl}(R) = \frac{4\Delta\tau R}{\pi\mu' v_{pl}} \equiv R/\dot{r}_c. \tag{9}$$

where we introduced the characteristic speed for the creep front propagation $\dot{r}_c = \pi\mu' v_{pl}/4\Delta\tau$. The numerical solution is close to the following expression (derived in Appendix A):

$$a(t) = R\sqrt{1 - t\dot{r}_c/R} \tag{10}$$

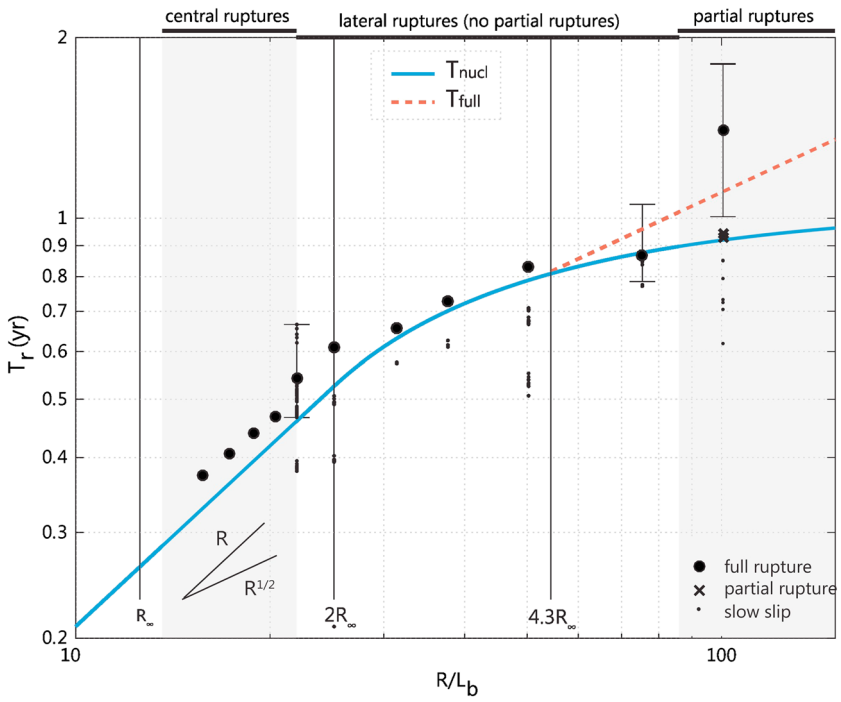

Figure 6. Scaling of T_r with R from the simulation (dots) and crack models (lines). Vertical lines mark the expected transition between regimes: aseismic to seismic (R_∞); central rupture to lateral ruptures ($2R_\infty$); onset of partial ruptures (4.3 R_∞), while the transitions observed in the simulations are marked at the top. T_{nucl} and T_{full} are calculated from equations (13) and (16).

where a is the distance of the crack from the center; equation (10) is shown by the dashed red line in Figure 5b. As the crack approaches the center, its propagation speed and slip velocity increase and eventually the latter reaches v_{dyn}. For the smallest asperities simulated, we see a brief elastodynamic event that decays as it expands outward before reaching the edge of the asperity (Figures 1, top and 7); these short rupture events are followed by a crack-like rupture expanding to the edge of the asperity. Since the moment of the second event is 1 to 2 orders of magnitude larger than the initial acceleration (as can be seen from the slip profiles in Figure 1), we consider the second event to be the repeating earthquake. This earthquake is well described as a constant stress drop crack propagating into the creeping region, where the stress is nearly uniform and equal to the steady state strength at v_{pl}, that is, $\tau_{ss}(v_{pl})$. The SIF of an elliptical crack in a uniform stress field is an increasing function of its size (e.g., Madariaga, 1977). Therefore, once nucleated the ruptures tend to accelerate and expand until they reach the edge of the asperity. As seen in the simulations, all accelerating events on faults nucleating from the center result in full ruptures, or they are followed by a full rupture within a short time interval (3–8 orders of magnitude shorter than the cycle duration, as seen in Figure 1), so that in this regime the recurrence interval is determined by T_{nucl}. The linear trend in T_r versus R (Figures 4 and 6) is in agreement with equation (9). For even smaller (aseismic) asperities, we expect a similar behavior, with v_{co} replaced by the slip speed during slow events. This speed, and hence $\Delta\tau$, decreases for smaller asperities, which explains why aseismic faults ($R/L_b < 12.5$) have shorter T_r than expected from equation (9) calculated with $\Delta\tau = \tau_{ss}(v_{pl}) - \tau_{ss}(v_{co})$ for seismic slip speeds (Figure 4).

We test the dependence of this scaling on rate-state parameters by running simulations with the same ratio R/R_∞ (where R_∞ is the nucleation radius, defined in equation (12)), fixed b, and variable a/b (Figure 7). We observe essentially the same behavior and the scaling predicted by equation (9) for a/b between 0.3 and 0.75. Larger a/b (0.85) gives rise to both *standard* ruptures (constant stress drop cracks), and elastodynamic events decaying as they expand, followed by slow crack-like ruptures. This pattern results in a period-2 cycle, with the duration of each subcycle consistent with equation (9), as discussed below.

We note that equation (9) has the same form as the recurrence interval estimated assuming a constant stress drop circular crack releasing an average slip $v_{pl}T_r = (16/7)\Delta\tau R/\mu'$, but it is a factor of 7/4 larger. This is consistent with the fact that a fraction of the nominal slip deficit $v_{pl}T_r$ is released by interseismic creep. There is

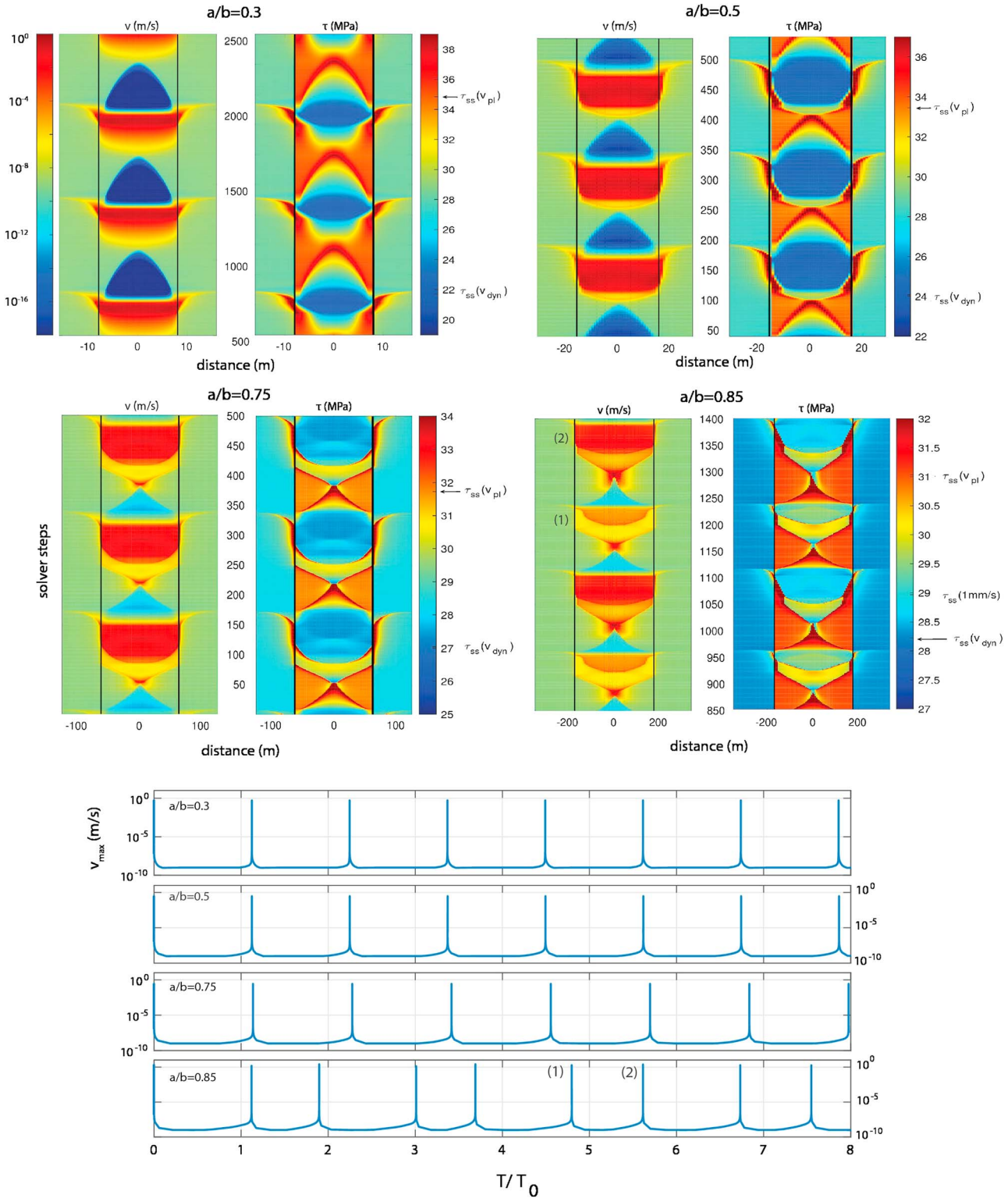

Figure 7. (top) Cycles for asperities with $R/R_\infty = 1.26$ and variable R and a/b, showing slip velocity and shear stress. For $a/b = 0.75$ and 0.85 the main quake (reaching the edge of the asperity) is preceded by brief fast slip. For $a/b = 0.85$, the velocity reached by the subsequent event (and determining the stress at the beginning of the following cycle) alternates between $\sim 10^{-4}$–10^{-3} m/s (event marked as 1) and ~0.1 m/s (event marked as 2). Fast events have a higher stress drop. (bottom) Maximum slip velocity versus time normalized by T_0 (from equation (13)). Note the period-2 cycle for $a/b = 0.85$, due to the alternation of seismic and slow events: fast events, with a higher stress drop, are followed by longer cycles.

also a conceptual difference between equation (9) and the classical argument. The latter is based on assumptions about the rupture occurring at the end of a cycle: it causes a stress drop $\Delta\tau$ and average slip $v_{pl}T_r$. In contrast, in our derivation these quantities are related to the interseismic phase: $v_{pl}T_r$ is the slip accumulated in the velocity-strengthening region during a cycle, and *not* necessarily equal to the coseismic slip; and $\Delta\tau$ is the stress increase between the end of the previous earthquake and steady state creep at the loading rate (equal to the stress drop of the *previous* event). While for period-1 cycles these are equivalent (since all events have the same $\Delta\tau$), the period-2 cycle for $a/b = 0.85$ gives us the opportunity to test these two hypotheses. Every other event is a slow earthquake and has lower stress drop. According to the classical argument, the longer recurrence intervals are expected to be followed by larger events (size predictable); while according to our argument, larger quakes should precede the longer recurrence interval, because the large stress drop will slow down subsequent creep propagation (time predictable). As shown in Figure 7, the slow creep events are followed by shorter cycles, consistent with equation (9); these cycles are about 1.4–1.6 times shorter than the cycles following standard ruptures. The predicted ratio of recurrence times with $\Delta\tau \sim \log(v_{co}/v_{pl})$, and v_{co} equal to 1 mm/s and 0.1 m/s for slow and fast ruptures is 1.3.

3.2. Onset of Lateral Ruptures

As predicted by a linear stability analysis (Ruina, 1983), a creeping crack with velocity-weakening friction becomes unstable above a critical dimension (nucleation size), so that lateral ruptures occur on asperities with a radius exceeding some size. Rubin and Ampuero (2005) estimated a critical dimension for 1-D cracks and aging law friction by treating the rupture as a constant stress drop crack with a SIF equal to the toughness determined from rate-state friction. Assuming steady state friction at seismic slip speeds immediately behind the crack tip, they estimate the maximum half length for stable propagation to be

$$L_\infty = \frac{1}{\pi}\left(\frac{b}{b-a}\right)^2 L_b \tag{11}$$

For a 2-D crack, we can assume that the rupture starts as a circular, penny-shaped crack within the creeping region of the asperity. For this geometry, we have $K_{\Delta\tau,p} = (2/\pi)K_{\Delta\tau,1-D}$, where the subscripts p (penny) and 1-D refer to the crack shape. The critical radius in three dimensions is thus

$$R_\infty = \frac{\pi}{4}\left(\frac{b}{b-a}\right)^2 L_b \tag{12}$$

As in the analysis of Rubin and Ampuero (2005), this is an upper limit for the nucleation dimension, valid at large slip velocities (e.g., $v \gg v_{pl}$). Since instabilities start within the creeping annulus in the velocity-weakening region (Figure 2), they can occur when the creep front has penetrated a distance $L_{pen} = 2R_\infty$. With the parameters used in our numerical simulations, $L_{pen} \sim 25L_b = 100$ m. If $R = 2R_\infty$ seismic rupture is expected to start at the center of the asperity, such that this length marks the transition between central and lateral ruptures, which in our simulations occurs at $R \simeq 22L_b = 88$ m, close to the $25L_b$ estimate.

At $R < R_\infty = 12.5L_b$, a constant stress drop crack expanding from the center encounters the edge of the asperity before reaching v_{dyn}. The slip accelerations observed as the creep front reaches the center (discussed in section 3.1) have a different geometry and nonuniform stress drop and might in principle reach v_{dyn} even on asperities with $R < R_\infty$; while this does not occur in our simulations, Chen and Lapusta (2009) found small events reaching seismic velocities at $R = 0.93R_\infty$. In our simulations, we find that the transition between aseismic and seismic slip occurs slightly above $R_\infty = 12.5L_b$ (between $R = 12.5L_b$ and $15.7L_b$, Figure 6).

To estimate the time to nucleation since the last rupture, we make use of the equation of motion of the creep front derived in Appendix A. Setting $a(t) = R - 2R_\infty$ in equation (10), and combining this result with equation (9), we obtain the nucleation time:

$$T_{nucl} = \begin{cases} R/\dot{r}_c & R < 2R_\infty \\ 4R_\infty\left(1 - R_\infty/R\right)/\dot{r}_c & R \geq 2R_\infty \end{cases} \tag{13}$$

This is shown by the blue line in Figure 6, which provides a close fit to the simulated recurrence times. For $R \gg R_\infty$, $T_{nucl} = 4R_\infty/\dot{r}_c$: the time to nucleation becomes independent of R. This is not surprising since this is approaching the 2-D limit, when the creep front propagation is independent of R. However, it would be

unphysical for the recurrence interval for full ruptures to be constant above a certain source radius. To understand earthquake cycles for $R \geq 2R_\infty$, we need to consider the conditions that determine rupture evolution and arrest, discussed in the following section.

3.3. Rupture Propagation and Arrest for $R \geq 2R_\infty$

Ruptures nucleating laterally have to propagate through the locked part of the asperity ($r < R - 2R_\infty$). As they propagate toward the center, they encounter lower stresses (since the stress imparted by creep decreases with distance from the asperity edge: equation (A5) and Figure B2). Therefore, ruptures may arrest within the locked region and not evolve into full ruptures (as previously observed by, e.g., Lapusta, 2003; Rice, 1993; Wu & Chen, 2014); the recurrence interval, taken as the time between full ruptures, will be longer than T_{nucl}. We estimate the time between full ruptures by requiring that the minimum value of the SIF during rupture propagation balance K_c (the toughness associated with a crack slipping at coseismic speeds; e.g., Werner & Rubin, 2013). In Appendix B we show that in this case equation (7) reduces to

$$K_I^* = K_c \tag{14}$$

where K_I^* is the minimum value of the SIF during propagation for a crack loaded by creep since the previous rupture. While an exact calculation of K_I^* requires knowing the shape of the crack as it evolves, dimensional arguments in Appendix B lead to

$$K_I^* = \frac{\mu' v_{pl} t}{\sqrt{R}} \phi, \tag{15}$$

where ϕ is a nondimensional factor related to the shape of the rupture and its position within the asperity.The minimum time for full ruptures is therefore

$$T_{full} = \frac{K_c}{\phi} \frac{\sqrt{R}}{\mu' v_{pl}}. \tag{16}$$

Assuming that the recurrence interval is close to T_{full}, we expect the scaling $T_r \sim \sqrt{R}$. This estimate of T_{full} ignores the influence of stress perturbations due to prior partial ruptures, which can be significant, and is therefore approximate. In order to estimate plausible values of T_{full}, in Appendix B we calculate ϕ numerically for a simplified rupture history, which gives $\phi = 0.76$. We point out that this value, and hence the minimum radius at which partial ruptures occur, is an order of magnitude estimate, since it greatly simplifies the shape and evolution of seismic ruptures: we discuss this issue in more detail below.

We calculate K_c in Appendix B, following Rubin and Ampuero (2005):

$$K_c = \sqrt{\mu' d_c b \sigma} \log\left(\frac{v_{co}\theta_i}{d_c}\right) \tag{17}$$

where θ_i is the state variable just outside the crack tip. Due to healing, this increases with time since the previous rupture. For the range of recurrence intervals considered, this has an effect of less than 10% on K_c, and for simplicity we set $\theta_i = 1$ year.

Partial ruptures can occur when $T_{nucl} < T_{full}$. Setting the second of equation (13) equal to equation (16), with $\Delta\tau = \tau_{ss}(v_{pl}) - \tau_{ss}(v_{co}) = (b-a)\sigma \log\left(v_{co}/v_{pl}\right)$, and with K_c given by equation (17), the critical radius for partial ruptures is the solution of

$$\sqrt{\frac{R_\infty}{R}}\left(1 - \frac{R_\infty}{R}\right) = \frac{\sqrt{\pi}}{8\phi} \frac{\log\left(v_{co}\theta_i/d_c\right)}{\log\left(v_{co}/v_{pl}\right)} \tag{18}$$

which, for the values of ϕ and θ_i used above, is satisfied by $R = 4.3R_\infty$. We note that equation (18) is a function of the ratio R/R_∞ and numerical constants, with only a weak dependence on the state variable and slip velocities. The dependence on stress drop and fracture energy (or, equivalently, rate-state parameters and σ) are included in the definition of R_∞. As for the previous transitions in rupture style, the ratio R/R_∞ defines the onset of partial ruptures. In the simulations, we find that the transition occurs between $R = 6R_\infty$ and $R = 8R_\infty$. This difference is most likely due to the approximations involved in estimating ϕ, as discussed below.

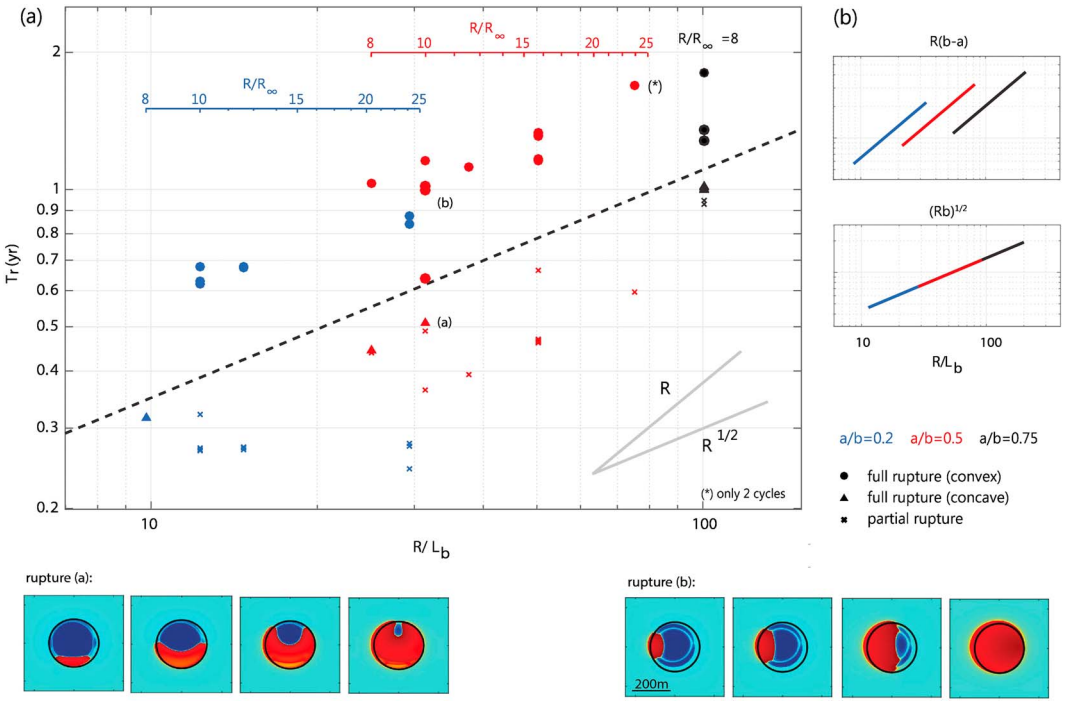

Figure 8. Scaling for asperities in the partial ruptures regime ($R/R_\infty \geq 8$), with fixed b and variable $b - a$. (a) Simulated cycles, with different rupture styles: partial ruptures (crosses), full ruptures that start with concave *horseshoe* shape (triangles), and convex full ruptures (circles). (b) Scaling expected from the classic argument: $T_r \sim R\Delta\tau \sim R(b-a)$ (top) and from the $K_I \geq K_c$ argument ($T_r \sim \sqrt{Rb}$) (bottom). The simulated events have different stress drops but the same fracture energy (from equation (A14)), so the $K_I \geq K_c$ argument predicts that they should fall on the same line.

3.4. Ruptures in the $R \gg R_\infty$ Regime

To test the criterion for full ruptures expressed by equation (16), we ran simulations with different parameters in the velocity-weakening region ($b - a = 0.01, 0.016$), shown in Figure 8. These values are chosen to cover a wide range of asperity dimensions R, while remaining in the large R/R_∞ regime and maintaining computational feasibility. The line defining T_{full} estimated above (equation (16)) separates most partial ruptures from full ruptures, as expected; but there are some exceptions. In some cases (mostly at $R/R_\infty = 8$, and a single event for $R/R_\infty = 10$), we observe convex ruptures starting with a *horseshoe* shape, which first propagate along the creeping annulus and then cover the center (triangles in Figure 8). Not surprisingly, the minimum time for full ruptures with ϕ estimated in Appendix B assuming an elliptical rupture (dotted line) fails to capture events with such a different rupture style. The disappearance of these events at larger R/R_∞ is probably due to this mode of propagation being determined by the creeping annulus, which becomes increasingly less significant (as a fraction of the asperity) as $R/R_\infty \to \infty$. Since all simulations have the same value of b (and hence fracture energy and K_c), we expect the recurrence interval to follow the scaling $\sqrt{R}$. On the other hand, the scaling derived from the classical argument assuming slip to be proportional to $v_{\text{pl}}T_r$ predicts $T_r \sim R\Delta\tau \sim R(b-a)$ (both scalings are shown graphically in Figure 8). In spite of the scatter in recurrence intervals, the plot suggests that simulations are better explained by the $K_I \geq K_c$ argument. While we chose small a/b values for computational reasons, we note that larger values of a/b (~ 0.9) are favored by laboratory experiments (Blanpied et al., 1998). For small asperities, we observe more complex slip histories for large a/b, and in particular $a/b = 0.85$ (Figure 7), in agreement with previous studies (Noda & Hori, 2014; Rubin & Ampuero, 2005); it is plausible that larger values of a/b would result in different behavior at large R/R_∞.

In summary, we expect the recurrence interval to scale as $T_r = T_{\text{nucl}} \sim R$ on small asperities ($R < 2R_\infty$), and approximately as $T_r = T_{\text{full}} \sim \sqrt{R}$ on larger asperities ($R \gtrsim 4.3R_\infty$), and with an intermediate exponent between the two (when $T_r \sim T_{\text{nucl}}$, but T_{nucl} scales sublinearly with R). This is in broad agreement with numerical simulations (Figure 6).

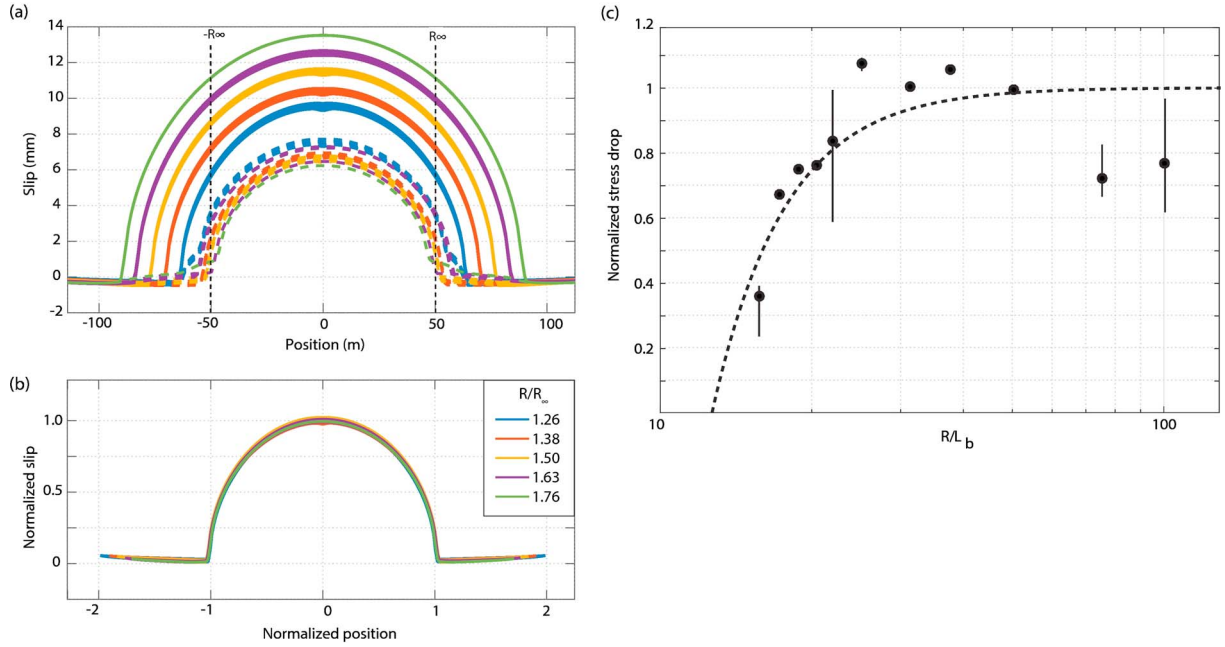

Figure 9. (a) Slip profiles for central ruptures with respect to the slip at the boundary at the onset of a rupture. Thick lines are the final slip distribution, dotted lines are the slip when the slip speed reaches v_{dyn} (i.e., at the start of an earthquake). (b) Slip profiles at the end of a seismic event, with lengths normalized by R. (c) Stress drops in the simulations (dots) and expected from equation (19), which takes into account the aseismic nucleation phase (dotted line). Stress drops are normalized by $\Delta\tau = 4.2$ MPa, which is the stress drop derived from the slip profile in the simulations and the expected limiting value as $R \gg R_\infty$.

4. Stress Drops and Scaling Between T_r and M_0

Crack models allow us to derive scaling relations between recurrence interval and source dimension. To understand the scaling with seismic moment ($M_0 \sim \mu\Delta\tau R^3$), we need to consider how stress drops scale with source radius. Figure 9b shows how the seismic moment scales with R in the simulations, obtained from equation (1) with M_0 given by integrating slip over the area during time steps with $v \geq v_{dyn}$ anywhere on the asperity. For the five smallest faults, an increase in stress drop with fault dimension is visible: this is due to a fraction of the seismic moment being released during the nucleation phase. Slip profiles during the seismic phase are well approximated by an elliptical crack with constant stress drop until the crack reaches the edge of the asperity and by a circular, penny-shaped crack at the end of the earthquake. This is consistent with a constant and spatially uniform stress drop during rupture growth and the same stress drop for earthquakes of different size as shown in Figure 9. However, Figure 9a shows that some of the slip is accumulated aseismically and thus does not contribute to the coseismic moment, defined as the moment released when $v \geq v_{dyn}$.

As the crack expands, the slip velocity increases. The crack starts slipping at seismic velocities once it reaches a finite size (R_∞). We can then calculate the moment released during the nucleation phase from the moment of a penny-shaped crack of radius R_∞. The coseismic moment is then given by

$$M_0 = M_{0tot} - M_{aseis} = \frac{16}{7}\Delta\tau\left(R^3 - R_\infty^3\right) \tag{19}$$

where the first term is the total moment released from the beginning of nucleation phase to the end of the earthquake. The ratio between seismic and total moment is $1 - \left(R_\infty/R\right)^3$, and it quickly approaches 1 (e.g., almost 90% of the moment is released coseismically for $R = 2R_\infty$, which corresponds to the transition between central and lateral ruptures). This indicates that the variation in stress drops is only expected to occur over a limited range of fault dimensions.

From the simulations, we find that crack reaches $v = v_{dyn}$ when the semimajor and minor axes reach 55 and 42 m, respectively, in the inplane and antiplane directions, close to our estimate of R_∞ (50 m). As expected, this dimension is approximately independent of asperity dimension R (Figure 9a). We estimate the total moment M_{0tot} directly from the slip profile: $M_{0tot} = \mu\pi SR^2/2$, where S is the slip at the center of the asperity. We find that

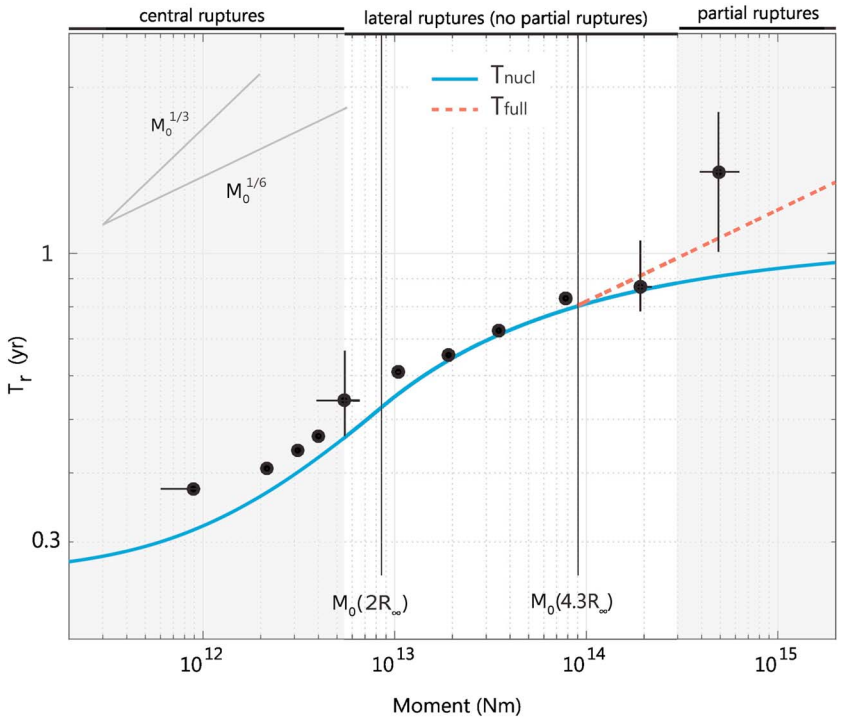

Figure 10. Scaling of T_r versus M_0. T_{nucl} and T_{full} from equations (13) and (16) and the seismic moment from equation (19). Transitions between rupture styles are determined by R/R_∞, not moment: depending on physical properties (a, b and σ) they would occur at different magnitude thresholds.

the scaling of M_{0tot} from the simulations is consistent with self-similarity, as expected from the fact that the slip profiles in Figure 9a have roughly the same shape. Furthermore, the scaling of M_0 with R is in agreement with equation (19). For the smallest fault ($R \sim 1.3R_\infty$), the stress drop estimated from M_0 is about 50% smaller than the stress drop estimated from M_{0tot}. Finally, we are in a position to combine the scaling of seismic moment with R and the dependence of T_{full} and T_{nucl} (equation (16) and (13)). This is shown in Figure 10. While some slight variations in the exponent are seen, we find that in the range $R_\infty < R \lesssim 4.3R_\infty$, the predicted trend is close to $T_r \sim M_0^{1/6}$. For $R \gtrsim 4.3R_\infty$, we expect $T_r \sim M_0^{1/6}$ scaling from constant stress drop and $T_{full} \sim \sqrt{R}$. This is the central result of the paper.

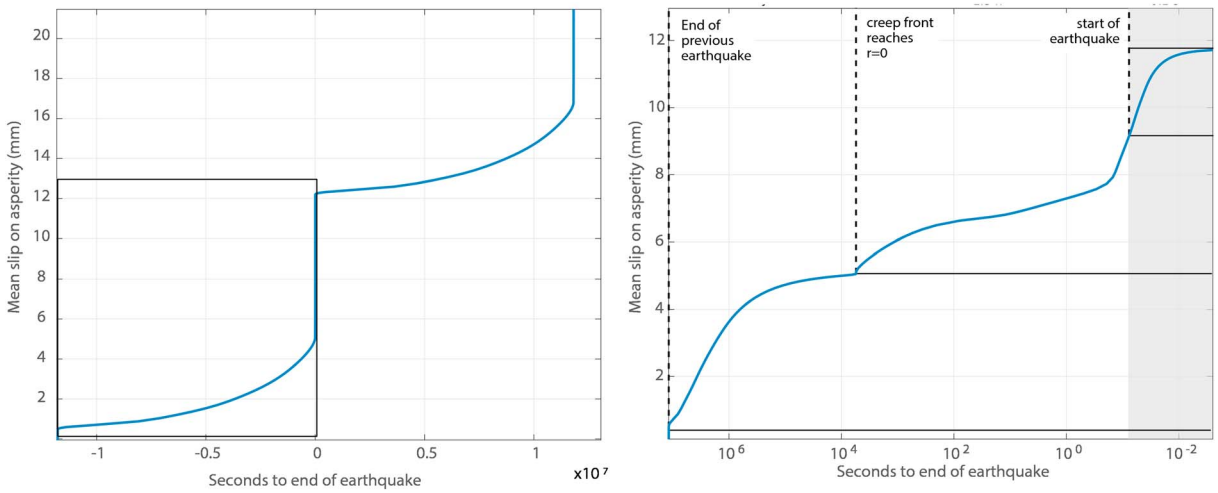

Figure 11. Average slip on the asperity during the cycle for the fault with $R = 16L_b$.

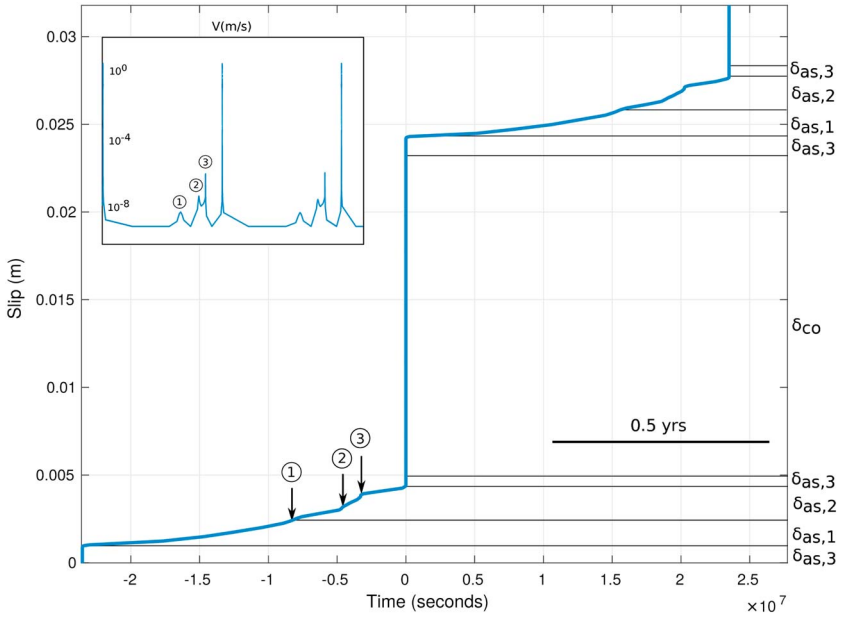

Figure 12. Average slip on the asperity during the cycle for the fault with $R = 50L_b$. δ_x are labeled as in equation (20).

5. Coseismic and Interseismic Slip Budget

Figures 11 and 12 show the contribution of seismic and aseismic slip on asperities with different R/R_∞. Aseismic stress release occurs in various phases of the seismic cycle: (1) during the interseismic period, as creep fronts propagate inward and parts of the asperities slip at a speed of the order of v_{pl}; (2) during aseismic slip episodes such as those shown in Figure 2; (3) during the acceleration and deceleration phase of an earthquake. The fraction of aseismic slip in phase (3) depends on the definition of *coseismic* slip velocity. The condition that the long-term slip rate on the asperity matches the loading rate can be expressed as follows:

$$S_{tot} = v_{pl} T_r = S_{seis} + S_{creep} + S_{nucl} + S_{post} \tag{20}$$

In Appendix C we derive analytical expressions for S_{creep} and S_{nucl} as a function of R/R_∞. The derivation of S_{nucl} is essentially equivalent to equation (19), and it is based on the observation that slip shown by the dotted elliptical profiles in Figure 9 accumulates between the time when the creep front reaches the center and the onset of the seismic phase (blue and yellow lines in the slip profiles in Figure 1); on the other hand, S_{creep}

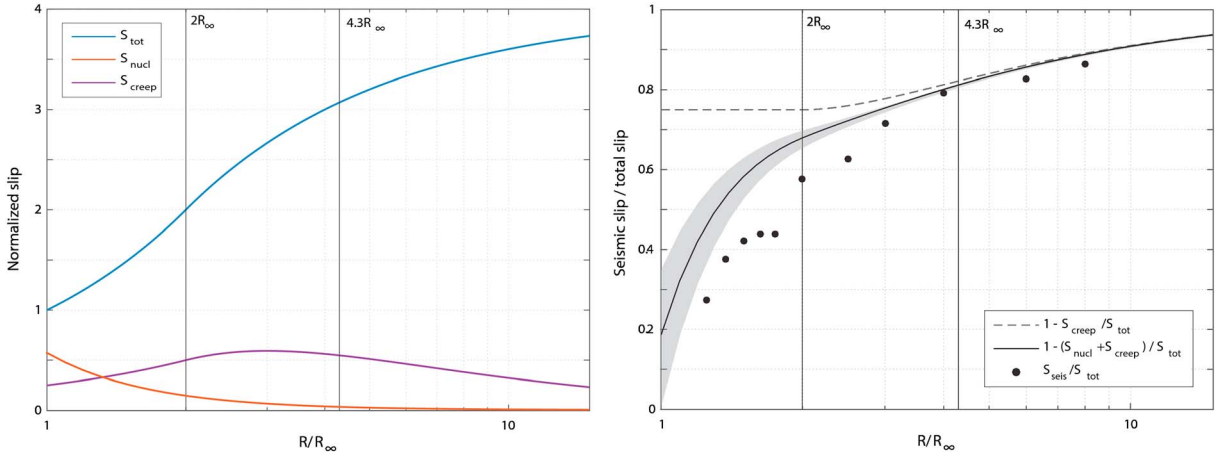

Figure 13. (left) Slip budget estimated from equations (C1), (C3), and (C4) normalized by the slip deficit on an asperity with $R = R_\infty$. (right) Fraction of seismic to total slip. Circles indicate the ratios observed in simulations; the black line is equation (21), assuming that $\Delta\tau$ in equation (C4) is the same as in equations (C1) and (C3). The gray area shows the range obtained allowing the stress drop during nucleation to differ from the stress increase during creep propagation ($\Delta\tau_{nucl} = [0.7-1.3]\ \Delta\tau_{creep}$).

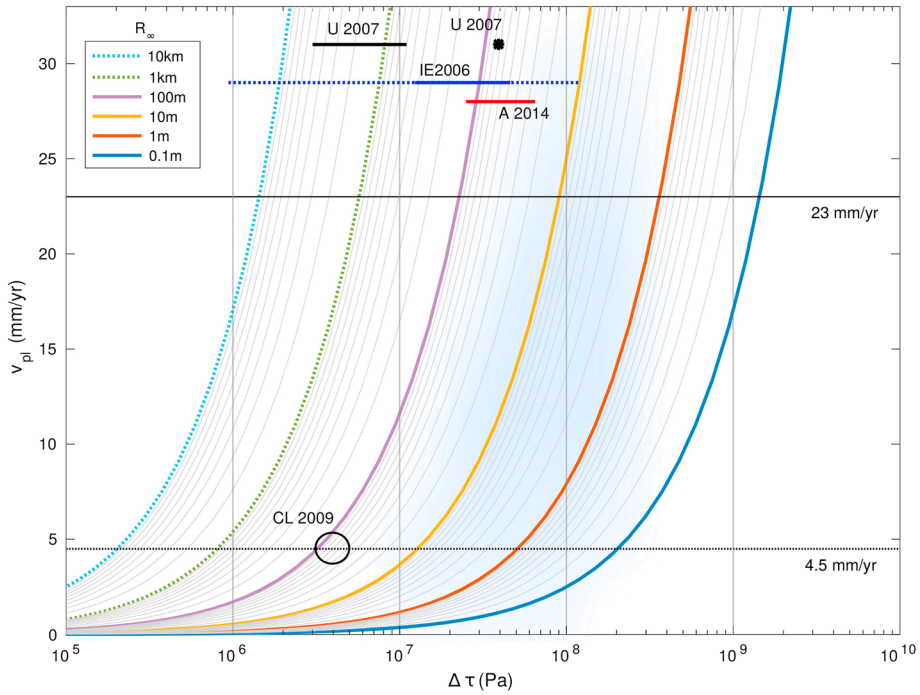

Figure 14. Combination of creep rate, stress drops, and nucleation lengths required to satisfy the scaling observed at Parkfield according to equation (28). Each line shows creep rate v_{pl} as a function of stress drop $\Delta\tau$ for a particular value of R_∞. The parameters chosen by Chen and Lapusta (2009) resulted in $R_\infty \sim 83$ m and $\Delta\tau \sim 4$ MPa, and the authors inferred a creep rate of 4.5 mm/year (smaller than the value of 23 mm/year used by Nadeau & Johnson, 1998). This interpretation is shown by the ellipse marked "CL2009." Bars at the top indicate seismological estimates of stress drops: Abercrombie, (2014; A2014, Parkfield, showing only well-constrained values); Imanishi & Ellsworth (2006; IE2006, Parkfield, with the entire range shown by the dotted line and 1 standard deviation by the thick line). Uchida et al. (2007, U2007, offshore Kamaishi, Japan, with the dot marking the value for the M_w4.9 repeater and the bar marking values estimated for smaller events). The shaded area indicates plausible values of parameter combinations, based on observed stress drops and nucleation lengths inferred from the small observed magnitudes (see text).

approximates the slip due to creeping at $v \sim v_{pl}$ (black lines in Figure 1). Simulations do not exhibit significant postseismic slip within the velocity-weakening asperity (Figures 11 and 12), consistent with results from spring slider simulations (Rubin & Ampuero, 2005; Segall, 2010). We therefore neglect this process as well as the contribution of transient aseismic slip episodes and partial ruptures for $R \gtrsim 4.3R_\infty$. Because of the latter assumption, these results are strictly valid only for $R \lesssim 4.3R_\infty$. Figure 13a shows predicted S_{tot}, S_{creep}, and S_{nucl} as a function of R/R_∞. As expected, S_{tot} has the same trend as T_r (Figure 6). The slip from interseismic creep is also proportional to T_{nucl} for $R < 2R_\infty$ (asperities on which the creep front reaches the center); in Appendix C we show that $S_{creep}/S_{tot} = 0.25$. For larger values of R, interseismic creep is confined to part of the asperity $r > R - 2R_\infty$, and its contribution decreases with R. Finally, the fraction of slip during the nucleation phase decreases monotonically with R. Combining these results we estimate the ratio of seismic to total slip as

$$\frac{S_{seis}}{S_{tot}} = 1 - \frac{S_{as}}{S_{tot}} = 1 - \frac{S_{creep} + S_{nucl}}{S_{tot}} \tag{21}$$

shown in Figure 13b. The ratio of seismic to aseismic slip derived from simple crack models provides a reasonable fit to the trend the simulations.

6. Discussion

Based on energy balance arguments and the scaling of SIFs with asperity dimension, we identified the following regimes:

1. $R < R_\infty$: asperities are aseismic.
2. $R_\infty < R < 2R_\infty$, creep completely erodes the asperity and seismic rupture nucleate from the center. The recurrence interval scales as $T_r \sim R$. Stress drops increase weakly with R.

3. $2R_\infty < R \lesssim 4.3R_\infty$: creep partially erodes the asperity before ruptures nucleate. When this occurs, the elastic energy accumulated from creep is sufficient for the rupture to propagate across the entire locked region, so that every nucleation results in a full rupture. The recurrence interval scales with $T_r \sim \sqrt{R}$.
4. $R \gtrsim 4.3R_\infty$: the energy required for a rupture to propagate through the locked region exceeds the energy required for nucleation, and partial ruptures occur. The recurrence interval of full ruptures is expected to scale as $T_r \sim \sqrt{R}$.

These results are broadly in agreement with Chen and Lapusta (2009), who found similar transition when increasing R with constant rate-state parameters, and Kato (2014). It is important to note that the transitions depend on the ratio R/R_∞, and not on the earthquake moment: the x axis in Figures 3 and 10 would take different values for different rate-state parameters or normal stress. The onset of partial ruptures at a sufficiently large value of R/R_∞ is essentially based on a comparison between the nucleation length and the overall asperity dimension. The fracture energy argument leading to $R_{nucl} = R_\infty$, proposed by Rubin and Ampuero (2005) and confirmed for circular asperities by Noda and Hori (2014), only applies for sufficiently large values of a/b (> 0.37). For smaller a/b, nucleation occurs on a length scale of $\sim 1.7L_b$ (Dieterich, 1992; Noda & Hori, 2014): therefore, in this case we expect all transitions to occur at values of R/R_∞ different from those predicted here. For example, this is consistent with the observation that $R/R_\infty = 8$ produces partial ruptures with $a/b = 0.5$, 0.75, but not with $a/b = 0.2$ (Figure 8). For $a/b = 0.2$, the nucleation radius ($R_{nucl} = 1.7L_b$) is larger than R_∞ by a factor of 1.4; the ratio of asperity radius to nucleation radius is therefore lower ($R/R_{nucl} = 5.7$). As expected, this asperity exhibits a behavior similar to the one with $a/b = 0.75$ and $R/R_\infty = 6$ (the second largest asperity in Figure 6), which does not have partial ruptures. But since such low values of a/b are not supported by lab experiments (e.g., Blanpied et al., 1998), in realistic cases we expect the ratio R/R_∞ to determine rupture behavior.

Interestingly, we find that the scaling between seismic moment and recurrence interval arises from different physical reasons depending on R. For small asperities, the recurrence interval scales linearly with dimension; in this range of R, it is the increase of $\Delta\sigma$ with R that gives rise to $T_r \sim M_0^{1/6}$ scaling. The nonconstant stress drop as R approaches the nucleation length is not surprising: crack models which predict constant $\Delta\tau$ assume a point source at $t = 0$, while the existence of a finite nucleation dimension breaks self-similarity as R approaches R_∞. For asperities with $R > 2R_\infty$, on the other hand, the relationship between T_r and M_0 is dominated by the $T_r \sim \sqrt{R}$ scaling, which originates from the dependence of the SIF on asperity dimension. In other words, we recover the observed scaling by considering seismic ruptures as releasing accumulated elastic energy rather than stress.

A simplification in our crack models is the neglect of inertia when balancing the SIF and fracture toughness. While this assumption is valid for modeling creep propagation (and hence T_{nucl}), when applied to seismic ruptures it may lead to an underestimation of T_{full}. An assumption behind our analysis is that the distribution of M_0 is dominated by variations in asperity dimension R, while spatial variations in physical properties play a secondary role. In reality, frictional parameters and normal stress are not necessarily uniform, and R_∞ can vary spatially. Assuming that such variations are independent of scale, this will generate scatter around the trend modeled here (since we found $T_r \sim M_0^{1/6}$ across a wide range of R/R_∞) but not affect the trend itself; since the results derived here imply that each *family* of asperities with given physical properties would fall on a $T_r \sim M_0^{1/6}$ line with a different proportionality constant. Additional heterogeneity with each asperity, due to fault roughness or variations in frictional and elastic properties, will also lead to more scatter in source properties and scaling. With this caveats in mind, below we discuss possible seismological observations predicted by our models.

6.1. Relating Observed Recurrence Intervals to $\Delta\tau$ and R_∞

The analytical expressions for T_{nucl}, T_{full} and M_0 (equations (13), (16), and (19) and Figure 10) allow us to estimate fault properties from the relationship between seismic moment and recurrence interval observed in nature. Nadeau and Johnson (1998) observed the relationship

$$\log_{10}(T_r) = 0.17 \log_{10}(M_0) + 6.0 \tag{22}$$

with T_r is the recurrence interval in seconds and M_0 the seismic moment in Newton meter. Chen et al. (2007) found that the same expression applies to repeating sequences in Taiwan and Japan, after rescaling the recurrence interval by the background creep rates in each location.

In the regime $R \geq 4.3R_\infty$, we obtain this scaling from M_0 and T_{full} (equations (1) and (16)): the constant of proportionality between T_r and $M_0^{1/6}$ is a function of fracture toughness K_c. On the other hand, for $R < 4.3$ the recurrence interval T_{nucl} as a function of M_0 is given by equations (13) and (19), which are functions of stress drop and nucleation length. We can reconcile the two by noting the relationship between K_c (equation (17)), R_∞ (equation (12)), and $\Delta\tau = \tau_{ss}(v_{pl}) - \tau_{ss}(v_{co})$, with τ_{ss} from equation (4):

$$\frac{K_c}{\Delta\tau} = \frac{\sqrt{d_c b\sigma\mu'}\log\left(v_{co}\theta_i/d_c\right)}{(b-a)\sigma\log\left(v_{co}/v_{pl}\right)} \approx 1.3\frac{\sqrt{d_c b\sigma\mu'}}{(b-a)\sigma} = 2.6\sqrt{R_\infty/\pi} \tag{23}$$

where we estimated the logarithmic terms as in section (3.3). Combining this expression with equation 16 and taking the ratio between T_{full} and $M_0^{1/6}$ (with equation (1) relating M_0 to R), we get

$$\frac{T_{full}}{M_0^{1/6}} = \frac{2.6(7/16)^{1/6}\sqrt{R_\infty/\pi}\Delta\tau^{5/6}}{\phi\mu' v_{pl}} \approx \frac{1.6\sqrt{R_\infty}\Delta\tau^{5/6}}{\mu' v_{pl}.} \tag{24}$$

where we used $\phi = 0.76$, as before. For $R < 4.3R_\infty$, the scaling is given by $T_{nucl}(R)$ and $M_0(R)$ (equations (13) and (19)). Figure 10 shows that these expressions yield a scaling close to $T_r \sim M_0^{1/6}$, but with some slight variations. To facilitate comparison with equation (22), we take the ratio between T_r and $M_0^{1/6}$:

$$\frac{T_{nucl}}{M_0^{1/6}} = \frac{\sqrt{R_\infty}}{\dot{\imath}_c\Delta\tau^{1/6}} f(R/R_\infty) \tag{25}$$

with

$$f(x) = \begin{cases} \left(\frac{7}{16}\right)^{1/6}\frac{x}{(x^3-1)^{1/6}} & R < 2R_\infty \\ \left(\frac{7}{16}\right)^{1/6}\frac{4(1-1/x)}{(x^3-1)^{1/6}} & R \geq 2R_\infty. \end{cases} \tag{26}$$

The function $f(R/R_\infty)$ quantifies the variations of T_{nucl} around a line of constant $M_0^{1/6}$ (see Figure 10). It is singular at $R = R_\infty$ (since the stress drop, and seismic moment, tend to 0); for R/R_∞ between 1.1 and 4.3, it ranges between 1.1 and 1.35, with an average value of 1.28. Therefore, we take $f(R/R_\infty) \approx 1.3$ and recalling that $\dot{\imath}_c = \pi\mu' v_{pl}/4\Delta\tau$, we can write

$$\frac{T_{nucl}}{M_0^{1/6}} \approx \frac{1.6\sqrt{R_\infty}\Delta\tau^{5/6}}{\mu' v_{pl}} \tag{27}$$

Note that equations (27) and (24) are the same, as expected from visual comparison of T_{nucl} (for $R < 4.3R_\infty$) and T_{full} in Figure 10. We are now in a position to relate the theoretical scalings with the observations. Setting equation (27) equal to equation (22), we find the constant of proportionality between $M_0^{1/6}$ and T_r:

$$\frac{T_r}{M_0^{1/6}} = \frac{1.6\sqrt{R_\infty}\Delta\tau^{5/6}}{\mu' v_{pl}} \approx 10^6 \tag{28}$$

Chen and Lapusta (2009) found that numerical simulations with $v_{pl} = 23$ mm/year (the creep rate inferred by Nadeau & Johnson, 1998, at Parkfield) produced shorter recurrence intervals than observed, and suggested that the long-term creep rate must be lower (4.5 mm/year). Equation (28) shows that the recurrence rate is determined by the creep rate, the nucleation length, and the stress drop. Combinations of these quantities which can explain the observed scaling are shown in Figure 14: each line indicates the background creep velocity required to explain the observed recurrence interval, as a function of $\Delta\tau$ and for a given value of R_∞. In spite of the approximations in equation (28), we recover the result from the numerical simulations by Chen and Lapusta (2009): their value of stress drop and R_∞ (~4 MPa and ~83 m, respectively) require $v_{pl} = 4.5$ mm/yr to explain the observed recurrence interval. They also noted that increasing d_c results in a longer recurrence interval, as can be seen in Figure 14; however, the nucleation length in this case becomes too large to explain the small magnitudes found at Parkfield (several events close to $M_w \sim 0$, Nadeau & Johnson, 1998).

It is plausible that the local creep rate near the repeaters may be lower or higher than 23 mm/year: as Nadeau and Johnson (1998) note, the geodetic inversion by Harris and Segall (1987), on which this value is based, shows variations between 4 and 35 mm/year near the repeater sequences. However, Chen et al. (2007) noted that sequences of repeating events in Taiwan and Japan follow the same scaling after renormalizing the recurrence interval by inferred creep rate in each region, and this implies that the creep rate would have been overestimated by the same factor in these locations. In alternative, a nucleation length of 10–100 m and a creep rate of about 23 mm/year can explain the observed T_r if stress drops are between 30 and 100 MPa, somewhat on the higher end of seismological values estimated for Parkfield repeaters (Abercrombie, 2014; Imanishi & Ellsworth, 2006) and in Japan (Uchida et al., 2007), shown in Figure 14. A smaller nucleation length ($\sim$ 1 m) may be more realistic considering that even smaller events have been observed at Parkfield ($M_w \lesssim -0.5$, e.g., Nadeau & Johnson, 1998; W. Ellsworth, private communication, 2018); this requires either very high stress drops ($\sim$400 MPa for $v_{pl} = 23$ mm/year), or a much lower creep rate or shear modulus; or a combination of these. The large uncertainties in estimated stress drops (see, e.g., Kaneko & Shearer, 2014, and section 6.2) and in the local creep rate make it challenging to determine which of these factors is dominant. Based on the available stress drops measurements, our preferred interpretation is that stress drops are in the 10–100 MPa range, and local creep rates are probably lower than 23 mm/year.

Equation (28) provides a physical interpretation for the scaling first observed by Nadeau and Johnson (1998), equation (22). A more commonly used form of this expression relates the interseismic slip $v_{pl}T_r$ to the seismic moment and can be obtained by multiplying both sides of equation (28) by v_{pl}. Based on the observations of Nadeau and Johnson (1998) at Parkfield, several studies have used small repeaters as creepmeters (e.g., Materna et al., 2018; Turner et al., 2015; Uchida et al., 2003, 2006). Our expression shows that estimating creep rates from the Parkfield observations is appropriate, as long as the nucleation length and stress drops are comparable to Parkfield. Since $\sqrt{R_\infty}$ scales inversely with stress drop (equation (23)), the dependence of T_r on $\Delta\tau$ is weak; we can see this from equation (16), or by combining equations (23) and (28):

$$\frac{T_r}{M_0^{1/6}} = \frac{2\sqrt{d_c b \sigma \mu'}}{\pi \mu' v_{pl} \Delta\tau^{1/6}} \tag{29}$$

Variations in normal stress, μ', d_c, or b, on the other hand, affect the recurrence interval more strongly. Therefore, the universal scaling observed by Chen et al. (2007) implies comparable fracture energy in the regions considered.

6.2. Observations Near the Nucleation Dimension

The existence of a finite nucleation dimension (R_∞) introduces a break in self-similarity. While the value of R_∞ estimated here is specific to rate-state friction with certain parameters, we expect this result to be general: since the stiffness of a constant stress drop crack is inversely proportional to its size, slip on cracks below a critical dimension is aseismic (e.g., Ruina, 1983).

Could this variation in stress drop be observed in nature? The main difference between a numerical simulation and real earthquakes is that with simulations we know the asperity dimension. Therefore, when estimating stress drops, the larger fraction of slip released aseismically on smaller asperities leads to lower stress drops. However, the existence of a finite nucleation dimension also shortens the distance a rupture propagates before reaching the edge of the asperity. Asperity dimension is commonly estimated from the rupture duration, inferred from the corner frequency and assuming an expanding circular crack with constant rupture velocity (Kaneko & Shearer, 2015; Madariaga, 1977; Sato & Hirasawa, 1973). For a rupture starting at $r = R_\infty$, the rupture duration will be shorter: in our simulations, it is proportional to $R - R_\infty$. This may lead to underestimation of the asperity dimension as $R \to R_\infty$, and overestimation of the stress drops. To further complicate matters, the rupture velocity is not constant during this phase (since the crack is still accelerating). Therefore, smaller asperities have lower average rupture velocity, which may partially counteract the previous effect. These results indicate that assuming a circular source expanding at constant velocity may lead to large biases in the estimation of source properties at dimensions near R_∞. We point out that the definition of *earthquake* used here (based on a velocity threshold) probably does not accurately reflect the way seismic ruptures are recorded, making it difficult to directly translate our results into observable variations in source properties. In fact, a similar study by Kato (2012b) found constant stress drops for ruptures nucleating at the center, the discrepancy most likely explained by the use of a lower velocity threshold (0.01 m/s), which resulted in part of

the nucleation phase (as defined in the present study) being included in the earthquake. Finally, we note that the final phase of the inward creep propagation for events that nucleate near the asperity center can result in peak velocities close to v_{dyn}, as described in section 3.1. In our pseudo-dynamic simulations, these events occurred minutes or hours before the main shock and were significantly smaller; they do however indicate that nucleation due to the convergence of a creep front may result in a more complex source-time function than a simple constant stress drop crack.

6.3. Transition Between Central and Lateral Ruptures

Circular sources propagating radially from the center are often used to infer source properties for small to moderate earthquakes. However, our results suggest that central ruptures only take place on asperities within a narrow range of dimensions ($R_\infty < R < 2R_\infty$) and should therefore be quite rare for repeating earthquakes in nature.

Studies of rupture directivity for moderate to small events (down to about $M3.0$) indicate a prevalence of unilateral ruptures, with no variation with magnitude (Abercrombie et al., 2017; Boatwright, 2007; Calderoni et al., 2015). A transition to central ruptures may occur at smaller magnitudes, for which estimating rupture directivity (or lack thereof) is particularly challenging.

6.4. Observations at Large R/R_∞

Finally, we estimated the minimum asperity radius that can host partial ruptures. While the exact dimension of the transition depends on the details of the asperity shape and assumptions in the derivation, the existence of such transition can be understood intuitively. Loading from the boundary of an asperity creates stress gradients within it, with lower stresses further away from the loading point. Stress increases everywhere with time, until an event can nucleate at the edge. If the asperity is large, the rupture will have to penetrate through a more extended region of lower stress, where it is more likely to arrest. This can also apply to other fault geometries: for example, Rice (1993),Werner and Rubin (2013), and Herrendorfer et al. (2015) found a similar transition in 2-D models of faults loaded by creep below the seismogenic zone, and Wu and Chen (2014) observed this transition in 2-D faults loaded from both ends. Similar concepts have been invoked to explain rupture arrest in laboratory experiments (Kammer et al., 2015). Kato (2014) also observed a similar transition in simulations at constant R and variable d_c, with low d_c resulting in partial ruptures. Moreover, he noted that the recurrence interval scales as $\sqrt{d_c}$, in agreement with the prediction from T_{full} in equation (B5) (since $K_c \sim \sqrt{d_c}$, as can be seen from equations (17).

We demonstrated that the recurrence interval of full ruptures for $R \gtrsim 4.3R_\infty$ is expected to scale as $T_r \sim \sqrt{R}$, leading to the moment scaling observed in nature for repeating events: it is likely that most of the observed repeaters are in this regime. An interesting question is how the occurrence of partial ruptures may affect the degree of periodicity of the system. Partial ruptures introduce variability in the stress field, not considered in our derivation: for example, a rupture may arrest in a low-stress region caused by a previous rupture (Lapusta, 2003) or be promoted by the stress concentrations outside its perimeter. These factors may affect not only the recurrence interval of full ruptures but also their slip evolution and observed waveforms, practically determining an upper bound to the characteristic behavior that defines a repeater. We note that the simulation with partial ruptures presents more variability in recurrence interval than those without (Figure 4); however, due to computational costs this simulation only produces a small number of full ruptures (three), and we cannot draw strong conclusions. Further studies are needed to verify whether asperities above a certain dimension lose the periodicity and characteristic behavior. Some indications of periodicity at large R/R_∞ can be inferred from the observed magnitude of repeaters, which can be as large as $M4.9 - 5.0$ (Chen et al., 2009; Uchida et al., 2012). Combined with the observation that most events above $M3.0$ are unilateral, and therefore in the regime where $R > 2R_\infty$, this suggests that asperities as large as $20R_\infty$ can have characteristic, quasi-periodic behavior. An alternative plausible explanation for this magnitude range may be regional variation in R_∞. However, more direct evidence comes from the observation of multiple families of repeaters with overlapping rupture areas (Uchida et al., 2007): the $M4.9$ Kamaishi (Japan) repeater experiences interseismic partial ruptures, mostly located near its edge (as expected from the crack models presented here). Given that most of these partial ruptures are between $2 < M < 3$, the Kamaishi repeater appears to be an example of a periodic earthquake many times larger than R_∞.

6.5. Slip Budget

Chen and Lapusta (2009) explained the scaling of T_r for small R/R_∞ by the increase of seismic to aseismic slip ratio with R, as seen in Figure 13; however, direct measurements of the slip partitioning at such small

magnitudes have proven challenging. Using borehole strainmeter records of small events on the San Andreas fault, Hawthorne et al. (2016) observed that the fraction of postseismic slip does not vary significantly as a function of magnitude (note that these observations could not determine whether slip occurred within or outside of the asperity). Based on our models, we expect aseismic slip on the asperity to occur mainly during the interseismic and the nucleation phase rather than postseismically. The propagation of the creep front on a circular fault is such that the creeping area grows approximately linearly with time (it would be exactly linear for the approximated equation of motion given by equation (10)); for a constant slip velocity behind the creep front, we thus expect a constant acceleration in moment. The total moment released by this process is not more than about a quarter of the total moment. The fractional contribution from the nucleation phase, on the other hand, can be arbitrarily large (Figure 13).

7. Conclusions

We developed crack models of circular asperities embedded in a creeping fault and found that they successfully reproduce the observed scaling between the recurrence interval and seismic moment: $T_r \sim M_0^{1/6}$. The temporal evolution of the creep front eroding an asperity is well fit by crack models, allowing us to quantify the contribution from aseismic slip during different phases of the seismic cycle.

Our models make specific prediction on the seismic behavior of asperities as a function of their dimension with respect to the nucleation radius R_∞. These findings are strictly valid for $0.3 < a/b < 0.75$: in this range, simulations with the same ratio R/R_∞ exhibit the same behavior. For smaller a/b, R_∞ should be replaced by $1.7L_b$, a better estimate of the nucleation half length; while for larger a/b, we observe similar scalings, but more variability in rupture style and recurrence interval between cycles. We identify a range of asperities over which ruptures nucleate from the center ($R_\infty < R < 2R_\infty$). Even though source models for events below $M5$ often assume central ruptures (e.g., Boatwright, 2007), we expect this behavior to be relatively rare due to the narrow range of R/R_∞ that exhibit this rupture style. We also note that the existence of a finite nucleation size introduces a break in self-similarity, which results in a decrease of stress drop with decreasing R. This effect leads to the $T_r \sim M_0^{1/6}$ scaling for small asperities.

For larger asperities, the same scaling is not due to variations in stress drop or to aseismic slip but to the relationship between SIF and radius. In particular, we find that an energy balance argument predicts that full ruptures are possible at $T_{\text{full}} \sim \sqrt{R}$, and hence $T_r \sim M_0^{1/6}$. According to our analysis, this criterion explains the recurrence interval for asperities above $\sim 4.3R_\infty$. We discuss observational evidence suggesting that the largest observed repeater (the $M4.9$ Kamaishi, Japan repeater) falls into this regime.

We show that the scaling across all regimes is to be approximated by $T_r = \frac{1.6\sqrt{R_\infty}\Delta\tau^{5/6}}{\mu' v_{\text{pl}}} M_0^{1/6}$. The dependence of this expression on the creep rate validates the use of small repeating earthquakes as creepmeters but also highlights the role of fault properties, which can affect the recurrence interval measured on different faults.

Appendix A: Creep Front Propagation

In order to slip at the loading velocity, the stress behind the crack tip must increase from the residual stress after an earthquake $\tau_{ss}(v_{co})$ to the steady state value at the creep rate $\tau_{ss}(v_{cr})$. In the simulations, we note that this is close to the loading rate v_{pl}, and for simplicity here we assume $v_{cr} = v_{pl}$. The crack can therefore be approximated by superimposing a stress-free end-driven crack and a crack with a spatially uniform negative stress drop $\Delta\tau = \tau_{ss}(v_{pl}) - \tau_{ss}(v_{co})$. Neglecting the contribution from fracture energy, the length of the crack $a(t)$ is determined by the condition that the total SIF vanishes, or

$$K_I(t, a) = K_{\Delta\tau}(a) \tag{A1}$$

where K_I is the SIF due to displacement at $a \geq R$, which we assume to grow linearly in time ($S = v_{pl}t$). The propagating creep front can be treated as an annular crack driven by edge displacement, which grows in response to an increase in the displacement boundary condition (analogous to the 2-D case analyzed by Mavrommatis et al., 2017). We consider an annular crack with outer radius R and inner radius $a(t)$.

A1. Annular Crack

For simplicity, throughout this work we employ results for SIFs for Mode-I cracks; for Mode-II or Mode-III cracks, the SIFs vary by a factor of order 1. Closed form solutions for the SIFs for an annular crack with fixed slip at $r = R$

are, to our knowledge, not available. Therefore, we estimate them numerically, and validate these solutions by comparing them to analytical results in the limits: $a \ll R$ and $a \to R$. Consider an annular crack with inner and outer radii a and R, subject to an axisymmetric stress $\tau(r)$. The SIF can be expressed as

$$K(t,a) = \int_a^R \tau(t,r)k(r)\mathrm{d}r \tag{A2}$$

where $k(r)$ is the SIF for a unit ring force at radius r. We evaluate $k(r)$ numerically, using the method introduced by Clements and Ang (1988). The stress distribution relevant for edge loading K_I is

$$\tau_I(r,t) = \tau_{\mathrm{rd}}(r)v_{\mathrm{pl}}t \tag{A3}$$

where τ_{rd} is the stress due to a unit ring dislocation at $r = R$ (Figure B2), with slip $\delta(r,t)$:

$$\delta(r,t) = \begin{cases} v_{\mathrm{pl}}t & r \geq R \\ 0 & r < R \end{cases} \tag{A4}$$

where t is the time since the last event and v_{pl} the plate velocity. The stress field inside a dislocation ring is given by (Kroupa, 1960):

$$\tau_{rd}(r) = \frac{\mu' v_{\mathrm{pl}}t}{\pi R}\frac{E(\rho)}{1-\rho^2} \tag{A5}$$

where $\rho = r/R$ and $E(k)$ is the complete elliptic integral of the second kind, which varies from 1 to $\pi/2$. It can be verified that this form gives the $1/x$ singularity in stress as $r \to R$ and reduces to $\tau_{rd} = \mu v_{\mathrm{pl}}t/2R$ at $r = 0$. We checked that the numerical solution of $K_I(a)$, approaches known solutions for the two limiting cases: the result from Selvadurai and Singh (1986) for $a \ll R$ and the 2-D solution for $a \to R$.

For $K_{\Delta\tau}$, we assume a uniform (and negative) stress drop (Figure 5), associated with increase in stress from that after dynamic rupture to steady state friction for creep at $v = v_{\mathrm{pl}}$, that is, $\Delta\tau = \tau_{\mathrm{ss}}(v_{\mathrm{pl}}) - \tau_{\mathrm{ss}}(v_{\mathrm{co}})$. We neglect the acceleration in slip speed (and hence decrease in $K_{\Delta\tau}$) as the slip front approaches the center (seen in the last snapshot in Figure 5). We use the approximate solution from Tada et al. (2000):

$$K_{\Delta\tau}(l) = \Delta\tau\sqrt{\frac{\pi l}{2}}\cdot F\left(\frac{l}{R}\right), \tag{A6}$$

with

$$F\left(\frac{l}{R}\right) = \frac{1 - 0.36l/R - 0.067(l/R)^2}{\sqrt{1-l/R}} \tag{A7}$$

and $l = R - a$. Using our numerical solution for $K_I(t,a)$ (obtained through equations (A2) and (A5)) and equation (A6) into equation (A1), we obtain the equation of motion for the creep front $a(t)$ shown in Figure 5.

A1.1. Calculating T_{nucl}

To get an analytical approximation for the time required for the creep front to reach the center of the asperity, we consider the limit $a/R \ll 1$. This is an estimate for the nucleation time on asperities with central ruptures. For K_I, we note that the SIF due to a displacement $\delta = S$ for $r \geq R$ and $\delta = 0$ for $r \leq a$ and zero stress in between is equivalent to that imposed by the boundary conditions $\delta = 0$ for $r \geq R$ and $\delta = -S$ for $r \leq a$, since the second state can be obtained from the first by subtracting a rigid body displacement, which generates no stresses. The stress field outside a dislocation ring of radius a and strength $-S = -v_{\mathrm{pl}}T_{\mathrm{nucl}}$ is (Kroupa, 1960)

$$\tau_{rd}(r) = \frac{\mu' S}{\pi a}\left[\frac{K(1/\rho)}{\rho} - \frac{\rho E(1/\rho)}{\rho^2 - 1}\right] \tag{A8}$$

where $\rho = r/a$ and $K(k)$ are the complete elliptic integral of the first kind. As $1/\rho \to 0$, this becomes

$$\tau_{\mathrm{rd}} = -\frac{v_{\mathrm{pl}}\mu'}{2a}\left(\frac{a}{r}\right)^3 T_{nucl} \tag{A9}$$

for $r > a$. Since we are estimating the time for the creep front to reach the center of the asperity, $a(T_{\mathrm{nucl}}) = 0$, we have $a/R \ll 1$ and can approximate the problem as an external crack of radius a. Since the displacements at $r \to \infty$ for an external crack subject to a field decaying sufficiently rapidly is null, the boundary condition $\delta(R) = 0$ is automatically satisfied in this limit. The SIF for an external crack subject to a stress field of the form $\tau(r) = \tau_0(r/a)^{-n}$ (as in equation (A9)) is given by Sih (1973), and for $n = 3$ reduces to

$$K_I = -\frac{2}{\sqrt{\pi}}\tau_0\sqrt{a} = -\frac{v_{\mathrm{pl}}\mu'}{\sqrt{\pi a}}T_{\mathrm{nucl}} \tag{A10}$$

The SIF for a constant stress drop (equation (A6)) in the limit $a/R \to 0$ is given by (Tada et al., 2000)

$$K_{\Delta\tau} = \frac{4\Delta\tau R}{\pi^{3/2}}\sqrt{\frac{1-a/R}{a}} \sim \frac{4\Delta\tau R}{\pi^{3/2}\sqrt{a}} \tag{A11}$$

Neglecting fracture energy, we set $K_I = K_{\Delta\tau}$ and obtain

$$t_0(R) = \frac{4R\Delta\tau}{\pi v_{\mathrm{pl}}\mu'} \tag{A12}$$

In the simulations, there is a delay between the arrival of the creep front and the onset of an earthquake; depending on R, this is of the order of seconds to hours (Figure 1), and thus negligible compared to the cycle duration. Therefore we take the nucleation time T_{nucl} equal to t_0. We can gain some insight into how the asperity dimension affects creep front propagation by considering the scaling of K_I and $K_{\Delta\tau}$. Rewriting equation (A10) in terms of the nondimensional length $\tilde{a} = a/R$, we see that $K_I \sim t/\sqrt{R}$, a result which, as we demonstrate in Appendix B is valid for a crack of any shape within the asperity. Similarly, equation (A6) shows that $K_{\Delta\tau} \sim \sqrt{R}$. Therefore, neglecting fracture energy and solving $K_I = K_{\Delta\tau}$ for a given value of $\tilde{a}$ results in $t \sim R$, so that when both distance and time are normalized by a factor proportional to R, the creep evolution curves collapse as in Figure 5. Figure 5 also shows that the normalized equation of motion is in agreement with the equation of motion calculated numerically.

A1.2. Effect of Fracture Energy

We include the effect of fracture energy by finding numerical solutions of

$$K_I + K_{\Delta\tau} = K_c \tag{A13}$$

where K_c is the fracture toughness, which is related to the fracture energy by equation (8). We employ the fracture energy for the aging law, in the no-healing approximation and constant slip velocity v_{in}, as given by (Rubin & Ampuero, 2005):

$$G_c = \frac{d_c b\sigma}{2}\left[\log\left(\frac{v_{\mathrm{in}}\theta_i}{d_c}\right)\right]^2 \tag{A14}$$

Since the crack is propagating into the locked region, we take $\theta_i = t + d_c/v_{\mathrm{co}}$ (from equation (3), with $\dot{\theta} \sim 1$ and $\theta(t=0) = d_c/v_{\mathrm{co}}$).

A2. An Approximate Solution

Here we derive an analytical form for the equation of motion of the creep front by treating the annular crack as an external circular crack and approximating the stress field imposed by the ring dislocation at $r = R$. The SIF for an external crack of radius a subject to uniform stress between $r = a$ and $r = R$ is (Sih, 1973)

$$K_{\Delta\tau} = \frac{2\sqrt{R}}{\sqrt{\pi}}\sqrt{\frac{1-\tilde{a}^2}{\tilde{a}}}\Delta\tau \tag{A15}$$

with $\tilde{a} = a/R$. Note that this differs from equation (A11) due to the use of an external crack, as opposed to an annular crack. Next we approximate K_I as due to a concentrated ring force at $r = R$, that is, $\tau(r) = P\delta(R)$,

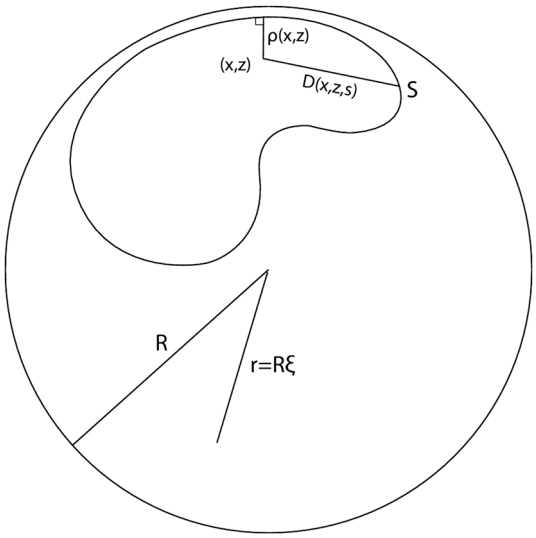

Figure B1. Example of a rupture propagating within the asperity, as presented in Rice (1989). The dimensions relevant to the calculation of SIFs (equation (B2)) are marked.

where P is a constant; $\delta(x)$ is the Dirac delta function, so that the ring force has the same form as the gradient of the imposed displacement (equation (A4)). This approximation assumes that the SIF is dominated by the singularity in the stress field; we note that for two-dimensional cracks, these two loading configurations produce exactly the same SIF ($K_I \sim \sqrt{l}$, where l is the distance between the loading point and the crack tip). The SIF in this case is Sih (1973)

$$K_I = \frac{2P}{\sqrt{\pi R}} \frac{1}{\sqrt{\tilde{a}(1-\tilde{a}^2)}} \tag{A16}$$

Setting $P = \alpha v_{pl} t$ (so that K_I is proportional to load point displacement), $K_{\Delta\tau} = K_I$ gives

$$a(t) = R\sqrt{1 - \frac{\alpha v_{pl} t}{R}} \tag{A17}$$

Further choosing $\alpha = \dot{\tau}_c / v_{pl}$ with $\dot{\tau}_c = \pi \mu' v_{pl} / 4\Delta\tau$ matches the condition given by equation (A12). This solution, although not rigorous, is close to the numerical result (Figure 5).

Appendix B: Estimating $T_{full}(R)$

Equation (7) considers the contribution of energy from elastic loading (K_I) as well as stress variations within the crack ($K_{\Delta\tau}$). In Appendix A, we saw that the propagation of the creep front is controlled by both terms. For a seismic rupture, the problem can be simplified by noting that we are considering a full seismic cycle, so that the net stress change is null. At $t = 0$ (just after a full rupture) the stress in the asperity is low: $\tau = \tau_{ss}(v_{co})$. Interseismically, creep outside the asperity raises the applied stress, while frictional strength changes as a result of healing as well as creeping on part of the asperity. These interseismic stress changes are reversed during seismic rupture, since the stress behind the seismic crack tip is $\tau = \tau_{ss}(v_{co})$. Therefore, we can set $K_{\Delta\tau} = 0$. For this argument to be strictly valid, we should account for stress changes on the asperity due to interseismic slip outside the hypothetical growing rupture. However, for simplicity, here we neglect the contribution from interseismic slip and assume that the asperity is entirely locked (a good approximation for $R \gg R_\infty$).

We estimate the SIF for a rupture nucleating at the edge of an asperity and propagating into the locked region. For a rupture in two dimensions, the SIF is a function of position along the front and it changes as the rupture grows. We consider the problem of a crack of an arbitrary shape growing within an asperity.

Rice (1989) developed a theory for calculating SIFs for two-dimensional cracks in a 3-D medium. For a crack subject to a stress field $\sigma(\mathbf{x})$, the SIF at position s along the rupture front is given by

$$K_I(s) = \int_{crack} k(\mathbf{x}; s)\sigma(\mathbf{x}) dA \tag{B1}$$

with

$$k(\mathbf{x}; s) = \frac{\sqrt{2\rho(\mathbf{x})} W(\mathbf{x}; s)}{\sqrt{\pi^3 D^2(\mathbf{x}; s)}} \tag{B2}$$

where ρ is the minimum distance between $\mathbf{x}$ and the edge of the crack, D the distance between $\mathbf{x}$ and point s along the crack, and $W(\rho, D)$ a nondimensional factor which takes into account the crack shape (see Figure B1). The terms $k(\mathbf{x}; s)$ are weight functions: they depend on the crack geometry and not on the applied stress. Note that they are a function of position along the front, and they vary as the rupture grows and potentially changes

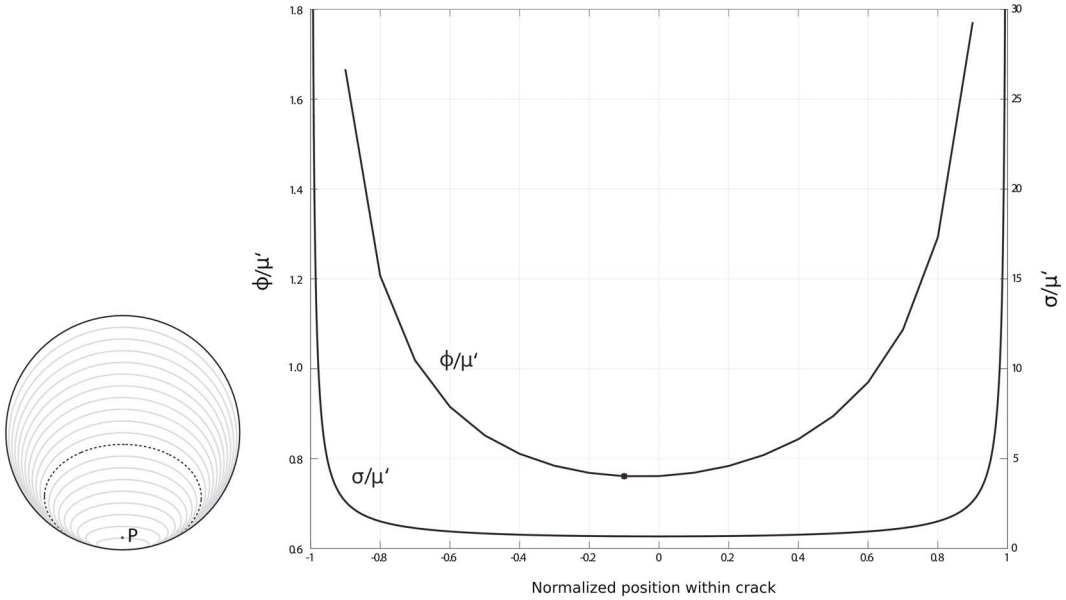

Figure B2. Stress intensity factor for a rupture nucleating on the side. (left) Sequence of elliptical cracks representing an idealized rupture history. Each ellipse is obtained by shifting the center along the vertical and matching the asperity curvature at the point of contact. (right) Stress intensity factor and stress field within the asperity. The SIF is calculated at point P (left panel). The minimum in ϕ (0.76) is marked with a circle, and it corresponds to the dotted ellipse in the left panel.

shape. The applied stress field $\sigma(\mathbf{x})$ is determined by the loading conditions on the asperity (i.e., interseismic loading) and is given by equation (A5). We can now write the SIF in terms of nondimensional variables $\xi = r/R$, $\tilde{\rho} \equiv \rho/R$ and $\tilde{D} \equiv D/R$:

$$K_I(s) = \frac{\mu' v_{\text{pl}} t}{\sqrt{R}} \phi(s) \tag{B3}$$

with

$$\phi(s) = \int \frac{\sqrt{2\tilde{\rho}(\mathbf{x})} W(\mathbf{x}; s)}{\sqrt{\pi^5} \tilde{D}(\mathbf{x}; s)^2} \frac{E(\xi)}{1-\xi^2} \mathrm{d}\tilde{A} \tag{B4}$$

where the integration is over the rescaled crack. Note that this term only depends on normalized lengths. As the crack grows and changes shape, the quantities $\tilde{\rho}$, $\tilde{D}$, and W vary. A rupture stops when $K_I(s) < K_c$ for all points s, which are still within the velocity-weakening region (or after penetrating a short distance into the VS region). For easier notation, we drop the dependence on s and we simply write $K_I < K_c$ when referring to this condition. A first-order scaling between the SIF and the asperity size can be derived by assuming that ϕ does not depend on R. This implies that rupture evolution is independent of asperity dimension, that is, the rupture history on an asperity is simply a rescaled version of the rupture history on an asperity of a different size. This can be considered an acceptable first-order approximation given that $\tilde{\rho}$, $\tilde{D}$ must always be in the range $[0, 2]$. By setting equation (B3) equal to K_c we obtain an estimate of the minimum recurrence interval:

$$T_{\text{full}} = \frac{K_c}{\phi} \frac{\sqrt{R}}{\mu' v_{\text{pl}}} \tag{B5}$$

and with constant ϕ we find a square root scaling between recurrence interval and source dimension.

To estimate realistic values of $T_{\text{full}}(R)$, we compute ϕ numerically for the rupture history shown in Figure B2, using the values of $W(\mathbf{x}; s)$ for an elliptical crack (Wang et al., 1998). In this case K varies along the rupture front. For the innermost point along the rupture front (P), we note that the ϕ has a nonmonotonic behavior as the rupture dimension grows: as P moves toward the center of the asperity, the stress field near P decreases and

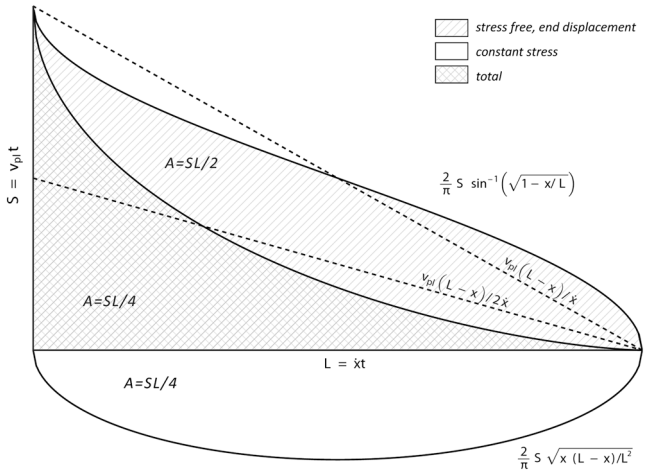

Figure C1. Slip profile for a stress-free crack with a displacement boundary condition; the constant stress drop crack which negates the SIF from the displacement-driven crack; and their combination. The dotted lines are the slip profiles assuming $v = 0$ ahead of the crack tip, and $v = v_{cr}$ behind, with $v_{cr} = v_{pl}$ and $v_{cr} = v_{pl}/2$.

so does $\phi(P)$. Note that the minimum of K occurs before P reaches the center of the asperity, since $\phi(P)$ does not depend only on the stress at P but also on the crack size (it increases with crack dimension). The minimum value of ϕ is 0.76.

The behavior of SIF at one point is not enough to determine whether the rupture stops. However, this simple model shows that ruptures starting at the edge of an asperity and propagating down a stress gradient may encounter a minimum SIF as they grow. This may lead to either partial seismic ruptures, or slow slip episodes, depending on whether the minimum is encountered before or after reaching the critical nucleation dimension.

Appendix C: Slip Budget

The slip deficit at the time of the first nucleation is given by $v_{pl}T_{nucl}$, and from equation (13) we have

$$S_{tot} = \begin{cases} \frac{4\Delta\tau}{\pi\mu'}R & R < 2R_\infty \\ \frac{16\Delta\tau}{\pi\mu'}R_\infty\left(1 - \frac{R_\infty}{R}\right) & R \geq 2R_\infty. \end{cases} \tag{C1}$$

In order to calculate the average slip from the propagation of the creep front, we need to know the slip profile for an annular crack analyzed in Appendix A. While there are simple expressions for this problem for 1-D cracks, there are no closed form solutions for the annular crack. Therefore, we use the following approximation: points ahead of the creep front do not slip, and points behind it accumulate slip at a constant rate v_{cr} (which, as discussed earlier, is of the order of v_{pl}). At the time of nucleation, the total slip at a point of radius r is $v_{cr}\left(T_{nucl} - t(r)\right)$, where $t(r)$ is the time when the front reached r. Approximating this time by the inverse of equation (A17), we obtain

$$s_{creep}(r) = \begin{cases} \frac{4\Delta\tau}{\pi\mu'}\frac{v_{cr}}{v_{pl}}\frac{r^2}{R} & R < 2R_\infty \\ \frac{4\Delta\tau}{\pi\mu'}\frac{v_{cr}}{v_{pl}}\frac{r^2-(R-2R_\infty)^2}{R} & R \geq 2R_\infty, \end{cases} \tag{C2}$$

We integrate this expression to obtain the average slip on the asperity at the time of nucleation:

$$S_{creep} = \begin{cases} \frac{2\Delta\tau}{\pi\mu'}\frac{v_{cr}}{v_{pl}}R & R < 2R_\infty \\ \frac{32\Delta\tau}{\pi\mu'}\frac{v_{cr}}{v_{pl}}\frac{R_\infty^2}{R}\left(1 - \frac{R_\infty}{R}\right)^2 & R \geq 2R_\infty. \end{cases} \tag{C3}$$

To constrain v_{cr}/v_{pl}, we consider the initial phase of the creep front propagation, when the annulus can be treated as a 1-D crack. As shown in Figure C1, the average slip within a stress-free crack driven by a slip boundary condition is the same as that of a linear slip profile given by constant slip rate $v_{cr} = v_{pl}$. However, the (negative) stress drop crack that cancels the SIF contributes negative slip, equal to half of the average slip for the stress-free crack. Therefore, we match the correct average slip in the annulus by setting $v_{cr} = v_{pl}/2$; v_{cr} should be thought of as an average slip velocity.

Finally, we consider the slip accumulated during the nucleation phase by treating the nucleating patch as constant stress drop crack of radius R_∞ (cf. section 4). The average slip due to this crack embedded within an asperity of radius R is given by

$$S_{nucl} = \frac{16\Delta\tau}{7\pi\mu'}\frac{R_\infty^3}{R^2} \tag{C4}$$

Assuming, as done before, that the stress drops during nucleation and creep propagation have the same absolute value, $\Delta\tau$ is the same in equations C1, C3, and C4, and these values differ only by factors containing R and R_∞.

Acknowledgments
We are grateful to Allan Rubin, Sylvain Barbot, and the Associate Editor for thoughtful reviews that significantly improved the manuscript. C. C. was supported by the German Academic Exchange Service (DAAD) with funds from the German Federal Ministry of Education and Research (BMBF) and the People Programme (Marie Curie Actions) of the European Union's Seventh Framework Programme (FP7/2007-2013) under REA grant agreement 605728, and NSF award 1620496. No new data was used in this study.

References

Abercrombie, R. E. (2014). Stress drops of repeating earthquakes on the San Andreas Fault at Parkfield. *Geophysical Research Letters*, *41*, 8784–8791. https://doi.org/10.1002/2014GL062079

Abercrombie, R. E., Poli, P., & Bannister, S. (2017). Earthquake directivity, orientation and stress drop within the subducting plate at the Hikurangi Margin, New Zealand. *Journal of Geophysical Research: Solid Earth*, *122*, 10,176–10,188. https://doi.org/10.1002/2017JB014935

Beeler, N. M., Lockner, D. L., & Hickman, S. H. (2001). A simple stick-slip and creep-slip model for repeating earthquakes and its implication for microearthquakes at Parkfield. *Bulletin of the Seismological Society of America*, *91*(6), 1797–1804.

Blanpied, M. L., Marone, C. J., Lockner, D. A., Byerlee, J. D., & King, D. P. (1998). *Journal of Geophysical Research*, *103*(B5), 9691–9712. https://doi.org/10.1029/98JB00162

Boatwright, J. (2007). The persistence of directivity in small earthquakes. *Bulletin of the Seismological Society of America*, *97*(6), 1850–1861. https://doi.org/10.1785/0120050228

Calderoni, G., Rovelli, A., Ben-Zion, Y., & Giovambattista, R. (2015). Along-strike rupture directivity of earthquakes of the 2009 L'Aquila, central Italy, seismic sequence. *Geophysical Journal International*, *203*(1), 399–415. https://doi.org/10.1093/gji/ggv275

Chen, T. (2012). Part I: Structure of central and southern Mexico from velocity and attenuation tomography; Part II: Physics of small repeating earthquakes (Ph.D. thesis), California Institute of Technology.

Chen, T., & Lapusta, N. (2009). Scaling of small repeating earthquakes explained by interaction of seismic and aseismic slip in a rate and state fault model. *Journal of Geophysical Research*, *114*, B01311. https://doi.org/10.1029/2008JB005749

Chen, K. H., Nadeau, R. M., & Rau, R. J. (2007). Towards a universal rule on the recurrence interval scaling of repeating earthquakes? *Geophysical Research Letters*, *34*, L16308. https://doi.org/10.1029/2007GL030554

Chen, K. H., Rau, R. J., & Hu, J. C. (2009). Variability of repeating earthquake behavior along the Longitudinal Valley fault zone of eastern Taiwan. *Journal of Geophysical Research*, *114*, B05306. https://doi.org/10.1029/2007JB005518

Clements, D. L., & Ang, W. T. (1988). Stress intensity factors for the circular annulus crack. *International Journal of Engineering Science*, *26*(4), 325–329. https://doi.org/10.1016/0020-7225(88)90112-7

Dieterich, J. H. (1978). Time-dependent friction and the mechanics of stick-slip. *Pure and Applied Geophysics*, *116*(4-5), 790–806. https://doi.org/10.1007/BF00876539

Dieterich, J. H. (1992). Earthquake nucleation on faults with rate- and state-dependent strength. *Tectonophysics*, *211*(1-4), 115–134. https://doi.org/10.1016/0040-1951(92)90055-B

Eshelby, J. (1957). Determination of the elastic field of an ellipsoidal inclusion, and related problems. *Proceedings of the Royal Society of London*, *241*, 376–396. https://doi.org/10.1098/rspa.1957.0133

Freund, L. B. (1990). *Dynamic Fracture Mechanics*, Cambridge Monographs on Mechanics. Cambridge, UK: Cambridge University Press. https://doi.org/10.1017/CBO9780511546761

Griffith, A. A. (1921). The phenomena of rupture and flow in solids. Philosophical Transactions of the Royal Society A: Mathematical. *Physical and Engineering Sciences*, *221*(582-593), 163–198. https://doi.org/10.1098/rsta.1921.0006

Harris, R. A., & Segall, P. (1987). Detection of a locked zone at depth on the Parkfield, California, segment of the San Andreas fault (USA). *Journal of Geophysical Research*, *92*(B8), 7945–7962. https://doi.org/10.1029/JB092iB08p07945

Hawthorne, J. C., Simons, M., & Ampuero, J. P. (2016). Estimates of aseismic slip associated with small earthquakes near San Juan Bautista, CA. *Journal of Geophysical Research: Solid Earth*, *121*, 8254–8275. https://doi.org/10.1002/2016JB013120

Herrendorfer, R., van Dinther, Y., Gerya, T., & Dalguer, L. A. (2015). Earthquake supercycle in subduction zones controlled by the width of the seismogenic zone. *Nature Geoscience*, *8*(6), 471–474. https://doi.org/10.1038/ngeo2427

Imanishi, K., & Ellsworth, W. L. (2006). Source scaling relationships of microearthquakes at Parkfield, CA, determined using the SAFOD pilot hole seismic array. In R. Abercrombie, et al. (Eds.), *Earthquakes: Radiated Energy and the Physics of Faulting* (vol. 170, pp. 81–90), Geophysical Monograph Series. Washington, DC: AGU. https://doi.org/10.1029/170GM10

Irwin, G. (1957). Analysis of stresses and strains near the end of a crack traversing a plate. *Journal of Applied Mechanics*, *24*, 361–364.

Kammer, D. S., Radiguet, M., Ampuero, J. P., & Molinari, J. F. (2015). Linear elastic fracture mechanics predicts the propagation distance of frictional slip. *Tribology Letters*, *57*(3), 1–10. https://doi.org/10.1007/s11249-014-0451-8

Kaneko, Y., & Shearer, P. M. (2014). Seismic source spectra and estimated stress drop derived from cohesive-zone models of circular subshear rupture. *Geophysical Journal International*, *197*(2), 1002–1015. https://doi.org/10.1093/gji/ggu030

Kaneko, Y., & Shearer, P. M. (2015). Variability of seismic source spectra, estimated stress drop, and radiated energy, derived from cohesive-zone models of symmetrical and asymmetrical circular and elliptical ruptures. *Journal of Geophysical Research: Solid Earth*, *120*, 1053–1079. https://doi.org/10.1002/2014JB011642

Kato, N. (2012a). Fracture energies at the rupture nucleation points of large interplate earthquakes. *Earth and Planetary Science Letters*, *353–354*, 190–197. https://doi.org/10.1016/j.epsl.2012.08.015

Kato, N. (2012b). Dependence of earthquake stress drop on critical slip-weakening distance. *Journal of Geophysical Research*, *117*, B01301. https://doi.org/10.1029/2011JB008359

Kato, N. (2014). Deterministic chaos in a simulated sequence of slip events on a single isolated asperity. *Geophysical Journal International*, *198*(2), 727–736. https://doi.org/10.1093/gji/ggu157

Kroupa, F. (1960). Circular edge dislocation loop. *Czechoslovak Journal of Physics*, *10*(4), 284–293. https://doi.org/10.1007/BF02033533

Lapusta, N. (2003). Nucleation and early seismic propagation of small and large events in a crustal earthquake model. *Journal of Geophysical Research*, *108*(B4), 2205. https://doi.org/10.1029/2001JB000793

Madariaga, R. (1977). High frequency radiation from crack (stress drop) models of earthquake faulting. *Geophysical Journal of the Royal Astronomical Society*, *51*(3), 625–651. https://doi.org/10.1111/j.1365-246$\times$.1977.tb04211.x

Materna, K., Taira, T., & Bürgmann, R. (2018). Aseismic transform fault slip at the Mendocino Triple Junction from characteristically repeating earthquakes. *Geophysical Research Letters*, *45*, 699–707. https://doi.org/10.1002/2017GL075899

Mavrommatis, A. P., Segall, P., & Johnson, K. M. (2017). A physical model for interseismic erosion of locked fault asperities. *Journal of Geophysical Research: Solid Earth*, *122*, 8326–8346. https://doi.org/10.1002/2017JB014533

Nadeau, R. M., & Johnson, L. R. (1998). Seismological studies at Parkfield VI: Moment release rates and estimates of source parameters for small repeating earthquakes. *Bulletin of the Seismological Society of America*, *88*(3), 790–814.

Noda, H., & Hori, T. (2014). Under what circumstances does a seismogenic patch produce aseismic transients in the later interseismic period? *Geophysical Research Letters*, *41*, 7477–7484. https://doi.org/10.1002/2014GL061676

Rice, J. (1989). Weight function theory for three-dimensional elastic crack analysis. In R. P. Wei & R. P. Gangloff (Eds.), *Fracture mechanics: Perspectives and directions (Twentieth Symposium), ASTM STP 1020*. Philadelphia: American Society for Testing and Materials, pp. 29–57.

Rice, J. R. (1993). Spatio-temporal complexity of slip on a fault. *Journal of Geophysical Research*, *98*(B6), 9885–9907. https://doi.org/10.1029/93JB00191

Rubin, A. M., & Ampuero, J. (2005). Earthquake nucleation on (aging) rate and state faults. *Journal of Geophysical Research*, *110*, B11312. https://doi.org/10.1029/2005JB003686

Ruina, A. (1983). Slip instability and state variable friction law. *Journal of Geophysical Research*, *88*(B12), 10,359–10,370. https://doi.org/10.1029/JB088iB12p10359

Sammis, C. G., & Rice, J. R. (2001). Repeating earthquakes as low-stress-drop events at a border between locked and creeping fault patches. *Bulletin of the Seismological Society of America*, *91*(3), 532–537. https://doi.org/10.1785/0120000075

Sato, T., & Hirasawa, T. (1973). Body wave spectra from propagating shear cracks. *Journal of Physics of the Earth*, *21*, 415–431. https://doi.org/10.4294/jpe1952.21.415

Segall, P. (2010). *Earthquake and volcano deformation* (517 pp.). Princeton, NJ: Princeton University Press.

Segall, P., & Bradley, A. M. (2012). Slow-slip evolves into megathrust earthquakes in 2D numerical simulations. *Geophysical Research Letters*, *39*, L18308. https://doi.org/10.1029/2012GL052811

Selvadurai, A. P. S., & Singh, B. M. (1986). The axial displacement of a disc inclusion embedded in a penny-shaped crack. *ZAMP Zeitschrift Fuer Angewandte Mathematik und Physik*, *37*(1), 64–77. https://doi.org/10.1007/BF00955519

Sih, G. C. (1973). *Handbook of stress-intensity factors*. Bethlehem Pa: Lehigh University.

Tada, H., Paris, P. C., & Irwin, G. R. (2000). *The stress analysis of cracks handbook* (58 pp). Hellertown PA: Del Research Corp. https://doi.org/10.1115/1.801535

Turner, R. C., Shirzaei, M., Nadeau, R. M., & Bürgmann, R. (2015). Slow and go: Pulsing slip rates on the creeping section of the San Andreas Fault. *Journal of Geophysical Research: Solid Earth*, *120*, 5940–5951. https://doi.org/10.1002/2015JB011998

Uchida, N., Matsuzawa, T., Ellsworth, W. L., Imanishi, K., Okada, T., & Hasegawa, A. (2007). Source parameters of a M4.8 and its accompanying repeating earthquakes off Kamaishi, NE Japan: Implications for the hierarchical structure of asperities and earthquake cycle. *Geophysical Research Letters*, *34*, L20313. https://doi.org/10.1029/2007GL031263

Uchida, N., Matsuzawa, T., Ellsworth, W. L., Imanishi, K., Shimamura, K., & Hasegawa, A. (2012). Source parameters of microearthquakes on an interplate asperity off Kamaishi, NE Japan over two earthquake cycles. *Geophysical Journal International*, *189*(2), 999–1014. https://doi.org/10.1111/j.1365-246$\times$.2012.05377.x

Uchida, N., Matsuzawa, T., Hasegawa, A., & Igarashi, T. (2003). Interplate quasi-static slip off Sanriku, NE Japan, estimated from repeating earthquakes. *Geophysical Research Letters*, *30*(15), 1801. https://doi.org/10.1029/2003GL017452

Uchida, N., Matsuzawa, T., Hirahara, S., & Hasegawa, A. (2006). Small repeating earthquakes and interplate creep around the 2005 Miyagi-oki earthquake (M=7.2). *Earth, Planets and Space*, *58*(12), 1577–1580. https://doi.org/10.1186/BF03352664

Wang, X., Lambert, S. B., & Glinka, G. (1998). Approximate weight functions for embedded elliptical cracks. *Engineering Fracture Mechanics*, *59*(3), 381–392. https://doi.org/10.1016/S0013-7944(97)00139-2

Werner, M., & Rubin, A. (2013). *Mechanical erosion of the seismogenic zone by creep from below on rate-and-state faults*. San Francisco, CA: AGU Fall Meeting Abstracts.

Wu, Y., & Chen, X. (2014). The scale-dependent slip pattern for a uniform fault model obeying the rate- and state-dependent friction law. *Journal of Geophysical Research: Solid Earth*, *119*, 4890–4906. https://doi.org/10.1002/2013JB010779